The Forsterite-Anorthite-Albite System at 5 kb Pressure

Kristen Rahilly

Submitted to the Department of Geosciences
of Smith College
in partial fulfillment
of the requirements for the degree of
Bachelor of Arts

John B. Brady, Honors Project Advisor

Acknowledgements

First I would like to thank my advisor John Brady, who patiently taught me all of the experimental techniques for this project. His dedication to advising me through this thesis and throughout my years at Smith has made me strive to be a better geologist.

I would like to thank Tony Morse at the University of Massachusetts at Amherst for providing all of the feldspar samples and for his advice on this project. Thank you also to Michael Jercinovic over at UMass for his help with last-minute carbon coating.

This project had a number of facets and I got assistance from many different departments at Smith. A big thank you to Greg Young and Dale Renfrow in the Center for Design and Fabrication for patiently helping me prepare and repair the materials needed for experiments. I'm also grateful to Dick Briggs and Judith Wopereis in the Biology Department for all of their help with the SEM and carbon coater. Also, the Engineering Department kindly lent their copy of LabView software for this project. I appreciated the advice from Mike Vollinger within the Geosciences Department as well as his dedication to driving my last three samples over to UMass to be carbon coated. The Smith Tomlinson Fund provided financial support.

Finally, I need to thank my family for their support and encouragement as well as my friends here at Smith for keeping this year fun and for keeping me balanced. Thank you to all of my geology major friends who make geology so much fun and to all of my professors at Smith who have inspired me!

Abstract

This study looked at three components of a typical syenite composition: forsterite (Mg_2SiO_4), anorthite ($CaAl_2SiO_8$), and albite ($NaAlSi_3O_8$). Various proportions of forsterite and either a pure albite, An_{48}, or An_{66} feldspar composition were mixed together to simulate a number of possible parent magma compositions. The compositional evolution of these parent magmas was experimentally investigated using a piston cylinder apparatus in order to simulate the conditions at 5 kbar pressure and across a range of possible temperatures. After holding the sample for 2-4 hours at the desired temperature and pressure in the piston cylinder, each sample composition was polished, carbon coated, and analyzed using a scanning electron microscope. Glass and mineral compositions were then plotted on a Fo-An-Ab ternary diagram to better constrain the cotectic at 5 kbar.

One of the main purposes of this study was to constrain the influence of Mg-rich mafic minerals (such as forsterite, the Mg end-member of olivine) on feldspar compositions at 5 kb pressure. Plotting the compositions of each sample mixture resulted in some interesting trends. Feldspar-rich samples that appear to be 100% glass do not plot on the expected bulk compositions. Instead, there is a distinct Na-rich nature to these glasses. As expected, any feldspar crystals that formed had a composition richer in Ca than that of the melt, resulting in glass compositions that are richer in Na and plot to the left of expected bulk compositions for that glass. Not all crystals that were seen compositionally in this way were physically evident on the SEM as Ca-rich crystals settled to the bottom of the less dense, Mg-rich magma. As these crystals were separated

by only a few millimeters from the top of the graphite chamber, the bulk composition of the system remained constant.

Differences exist between this study's Fo-An-Ab ternary diagram at 5 kbar with the Fa-An-Ab system at the same pressure by Morse et al. (2007). The addition of a more Mg-rich mafic mineral (forsterite) in place of fayalite pushed the cotectic closer to the feldspar join. Consequentially, the forsterite-saturated plagioclase compositions can exist across a wider temperature range (approximately 250°C) than fayalite-saturated plagioclase (27°C) (Morse et al., 2007).

Table of Contents

Index of Figures and Tables

Figures from Chapters 1-6

Tables from Chapters 1-6

Chapter 1: Important Petrological Concepts

Compositional evolution of magmas

By studying the mineralogy and texture of an igneous rock, it is possible to deduce much about the history of its formation. However, by considering the possible compositions of parent magmas, we are able to understand better the compositional evolution that has produced a specific mineralogy. In igneous petrology, a number of petrological questions are pertinent to the description of a rock composition. What does mineralogy tell us of possible parent magmas? How primitive or evolved is the rock in terms of crystallization from an original magma? What is the ratio of felsic to mafic components and what does this tell us of the origin of formation?

Many of these questions can be answered using Bowen's Reaction Series, which conceptually shows the progressive crystallization of mafic and felsic components from most primitive to most evolved compositions **(**Figure 1**)** (Blatt and Tracy, 1996, p. 40). This diagram gives a general, conceptual introduction to how the compositional evolution of a magma is dependent on a number of factors. On the left, mafic side of the diagram is the "discontinuous series". The progression of minerals shown here can be independently dependent on pressure, temperature, and availability of silica (Blatt and Tracy, 1996, p. 42). For example, just as the amount of silica within a system can determine whether the resulting igneous rock is classified as "mafic", "intermediate", or "felsic", the availability of silica determines which minerals are able to crystallize. For example, olivine [$(Mg,Fe)_2SiO_4$] requires a smaller weight percent silica than the Mg-rich pyroxene enstatite [$Mg_2Si_2O_6$]. On the right side of Figure 1 is the "continuous series", where the

pressure-temperature variance spans the solid-solution end-members of plagioclase: the Ca-rich member anorthite ($CaAl_2Si_2O_8$) and the Na-rich member albite ($NaAlSi_3O_8$).

The most important general concept from Bowen's Reaction Series (Figure 1) is that a mafic, undifferentiated igneous rock can become more compositionally evolved through fractional crystallization dependent on the pressures, temperature, and original compositions that define them.

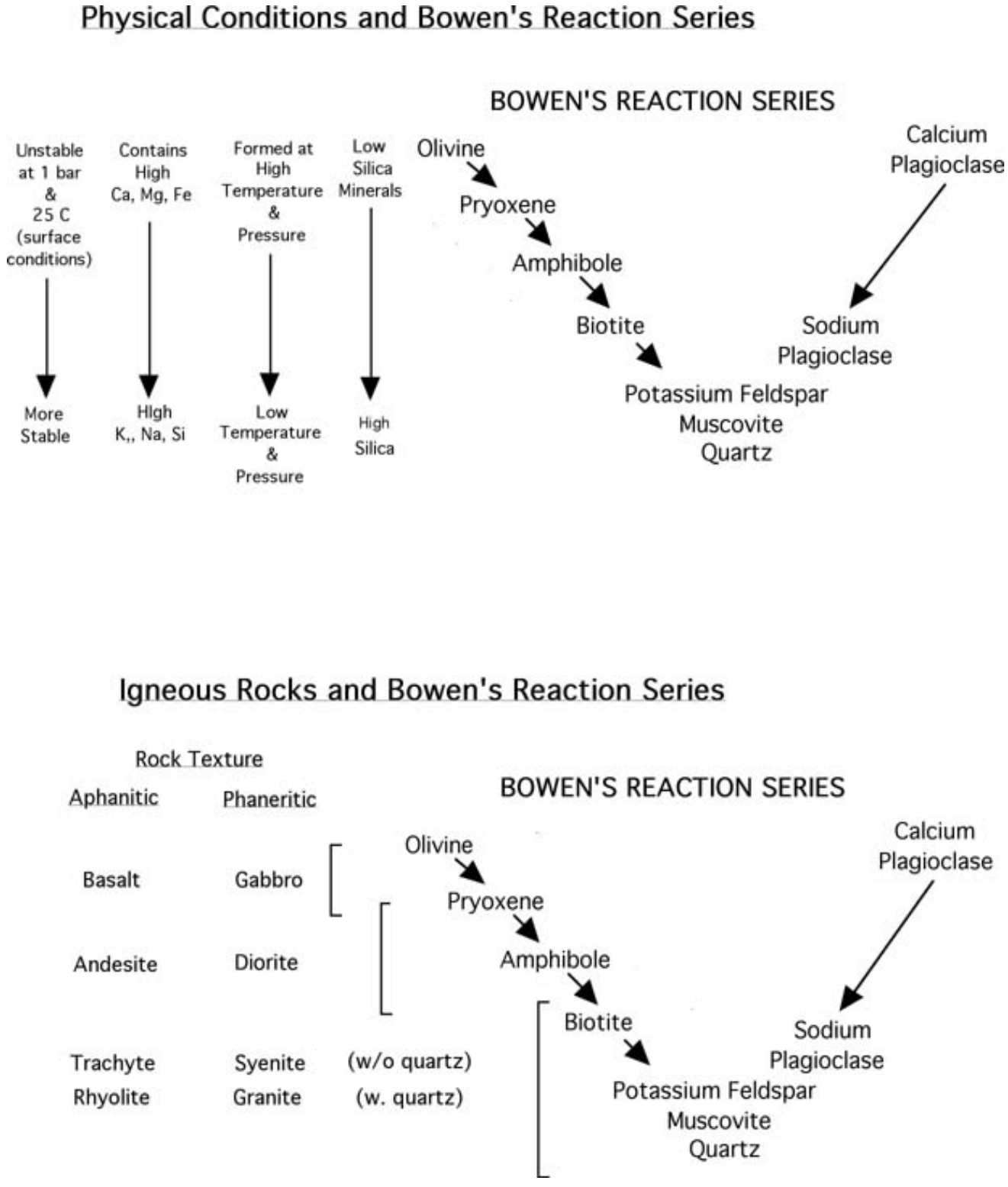

Figure 1. Physical conditions that play a part in the progression of crystallization according to Bowen's Reaction Series (A) and the igneous rocks and textures that result from each stage of the series (B). Both images from: http://www.skidmore.edu/~jthomas/fairlysimpleexcercieses/brs.html.

Effects of Temperature and Pressure on Compositional Evolution

In this study, pressure was kept at a constant 5 kb while temperature varied for each experimental run. A pressure of 5 kb was chosen as prescribed by Morse et al. (2007) and following a previous study completed by Morse et al. (2004) in order to simulate better the conditions at which natural syenites form. This pressure of 5 kb (0.5 GPa) is experienced by rocks approximately 18 km below the surface (Winter, 2001, p.119). Due to advances in technology and the further evolution of the basic piston-cylinder setup first used by Boyd and England (1962), we are able to simulate conditions at realistic depths and temperatures for intrusive igneous rocks. This is quite an improvement over the 1 atmosphere limitation imposed on Schairer and Yoder (1967).

The direct effects that pressure has on compositional evolution can be described at a basic level through changes of the total energy content within a chemical system (Winter, 2001, p. 76). This concept is referred to as "Gibbs free energy" (G) and can be described (Eq.1) in terms of chemical reactions of the form reactants → products:

(Eq.1) $\Delta G = \Sigma(n_{products}G_{products} - n_{reactants}G_{reactants})$, where ΔG is the change in Gibbs free energy, n is the stoichiometric coefficient for each reaction phase, and G is the Gibbs free energy for each phase.

In his basic explanation of the significance of "G", Winter (2001) concludes that "stable forms of a chemical system are those with the minimum possible Gibbs free energy for the given conditions" (p.76) and thus "the side of a reaction equation with lowest G under

a given set of conditions is the most stable" (p. 80). In order to illustrate the "given conditions" that are important in this study, Eq.2 represents the change in free energy ($d\Delta G$), volume (ΔV), and entropy (ΔS) due to progression of the reaction, and the finite changes possible for pressure (dP) and temperature (dT):

(Eq.2) $$d\Delta G = \Delta V dP - \Delta S dT$$

In other words, Eq.2 means that changes in the amount of free energy within a system ($d\Delta G$) due to a reaction are dependent on the state changes pressure and temperature. Figure 2 further shows that the temperature at which a solid melts or a liquid crystallizes is directly dependent on the total pressure on the system.

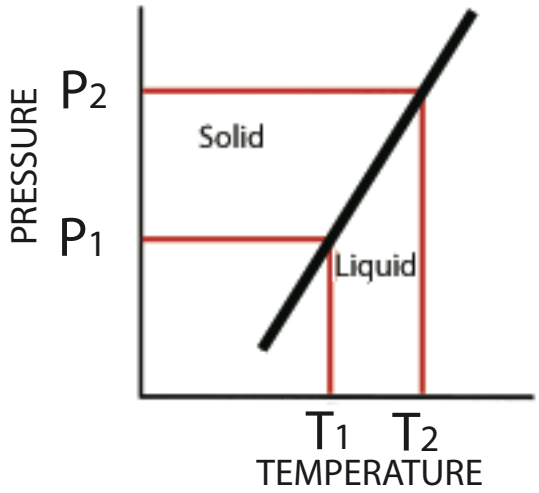

Figure 2. Pressure-Temperature diagram from Winter (2001, p. 119) showing the increase in melting point with increasing pressure.

In terms of state change, an increase or decrease in pressure and/or temperature results in a change in the amount of free energy within the system ($d\Delta G$). As illustrated by Eq.1, if the products of this state change have less free energy than the reactants, the reaction will

move towards the reactant phase in order to minimize G and vice versa. In the reaction ($G_{liquid} - G_{solid}$), the system in question will remain solid if $\Delta G > 0$ and will melt if $\Delta G < 0$. If both phases are equally stable, however, the $\Delta G = 0$ (Winter, 2001, p. 81).

The crystallization or melting of intrusive igneous rocks can be used as an example of this concept. Lindsley (1967) calculated that at 10 kb pressure, pure albite ($NaAl_3O_8$) will melt at approximately 1230° C, meaning that the system moves towards the liquid phase and $\Delta G < 0$. In order for the same albite composition to melt at an increase in pressure to 20 kb, the temperature at which the liquid phase exists must also increase in order to keep the resulting ΔG as small as possible. With a small ΔG, $G_{liquid} < G_{solid}$ and the reaction will proceed towards the liquid phase. With the 5 kb pressure used in this study, it took a lower temperature input than that needed at 20 kb to reach the point at which ΔG is negative and the phase could change from solid to liquid.

Chapter 2: Study Questions, Objectives, and Materials

An Introduction to Syenites

Interest in this project stemmed from a proposal for a five-college, cooperative experimental study to investigate the origin of syenites and trachytes (Morse et al., 2007). At its most basic description, a syenite is an intrusive, highly alkaline igneous rock that, unlike granite, is undersaturated in silica (Morse et al., 2007). The felsic components of typical syenites are usually alkali and plagioclase feldspars while mafic minerals may include olivine, hornblende, biotite, or augite (Carmichael, Turner, and Verhoogen, 1974, pp.39). Within the overarching syenite classification there are a wide range of possible compositions (Bhattacharya and Kar, 2005; Carmichael, Turner, and Verhoogen, 1974). As a more general category, syenites can vary in the ratio of mafic to felsic components, determining whether classification as a mafic or felsic syenite would be suitable (Bhattacharya and Kar, 2005). Further winnowing down of the classification is dependent upon enrichment in a certain mineral relative to other components. The location of syenites in the IUGS classification diagram of igneous rocks (Figure 3) clearly shows these possible syenite composition variations.

Figure 4 is a compilation of various syenite compositions from the Gardar Province of South Greenland ("Gardar"), the Kiglapait Intrusion of Labrador ("KI"), the Sybille monzosyenite intrusion of the Laramie anorthosite complex in Wyoming ("SYB"), and syenites from Gough Island in the South Atlantic Ocean ("Gough") (Morse et al., 2007). The interesting thing about this figure is that the syenites studied have a wide variety of Mg# [Mg/(Mg*Fe)] that differ greatly from the average composition of

syenites (SY) determined by Le Maitre (1976). When paired with feldspar compositions, Figure 4 seems to stray from the basic concepts of igneous rock evolution as seen in Bowen's Reaction Series (Figure 1).

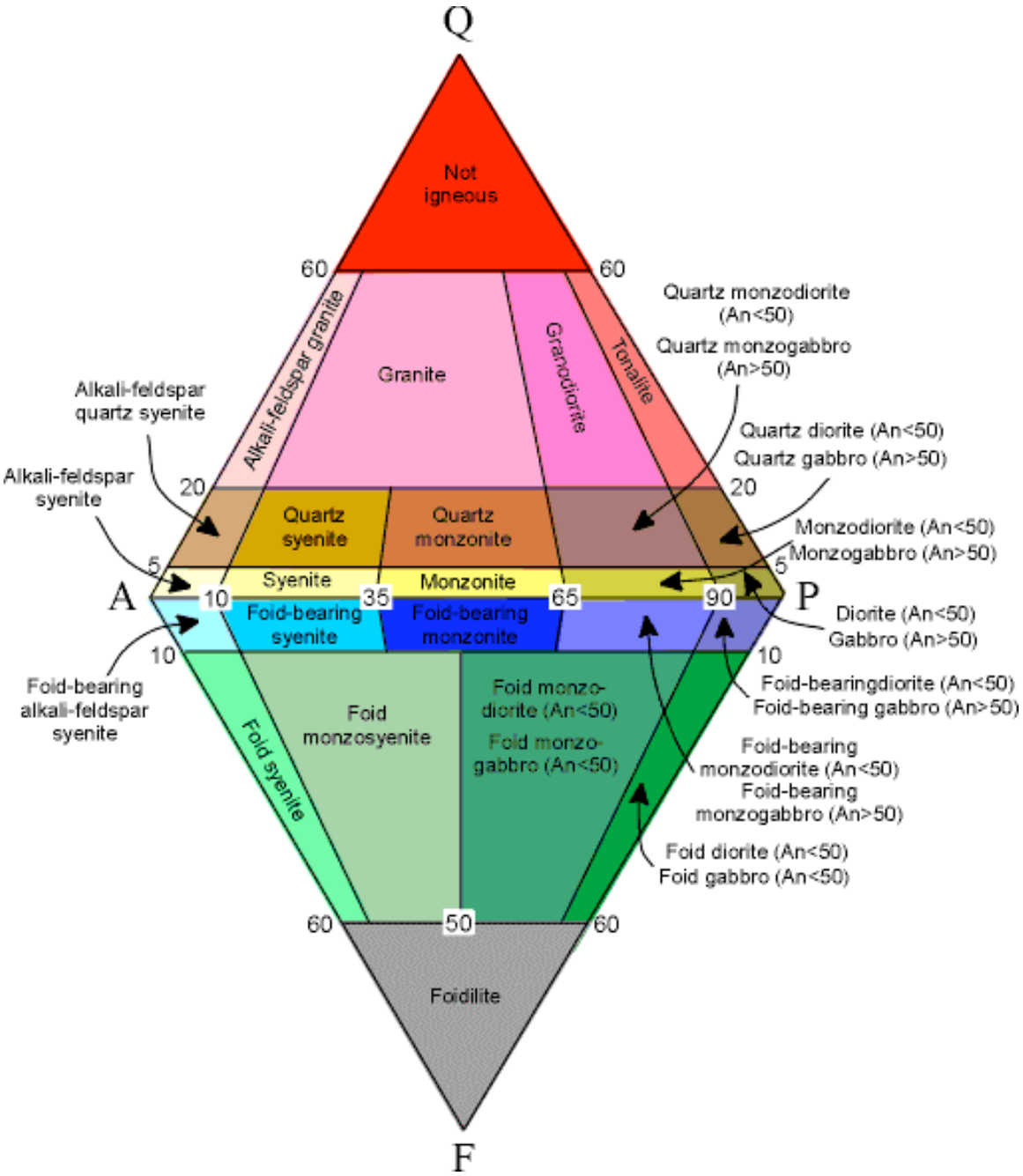

Figure 3. The IUGS classification of igneous rocks based on the relative proportions of quartz (Q), plagioclase feldspar (P), alkali feldspar (A), and feldspathoids (F).

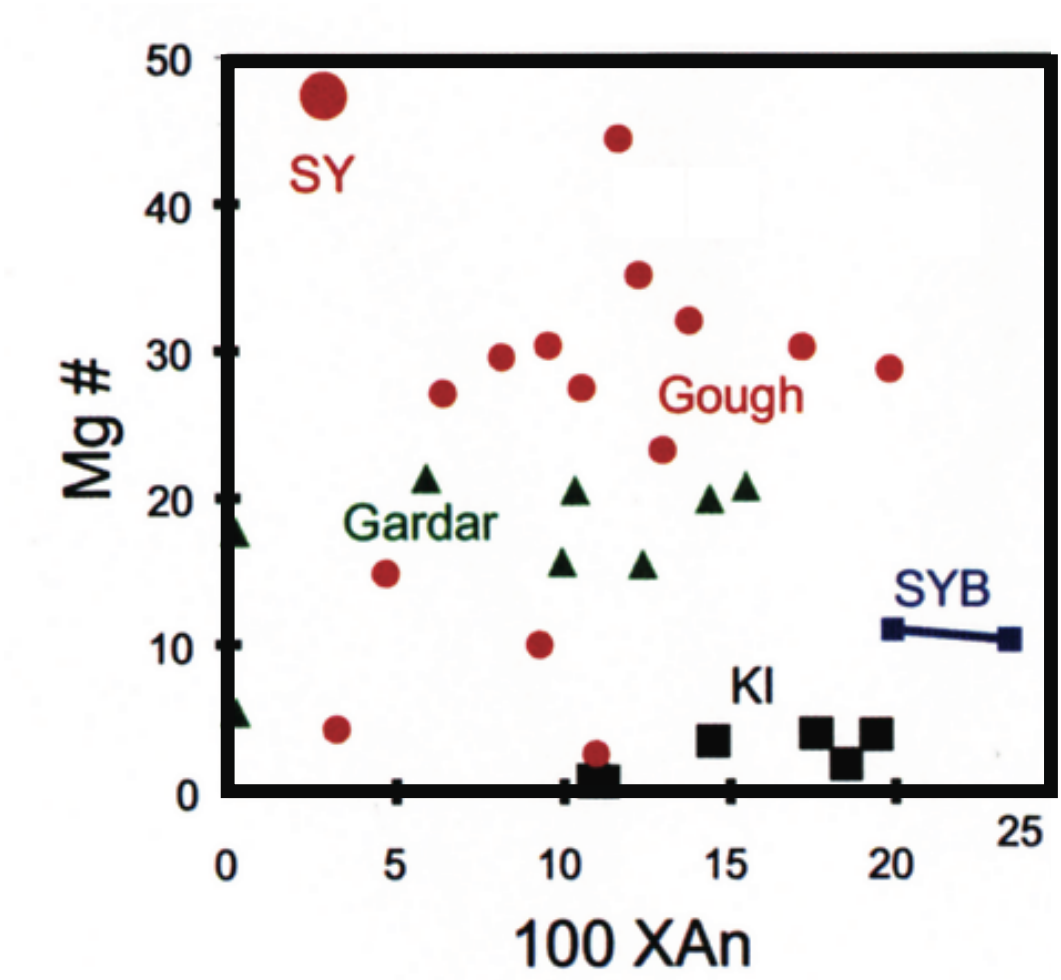

Figure 4. Compilation by Morse et al. (2007) of syenite compositions from a number of localities relating Mg # [Mg/(Mg*Fe)] and feldspar composition (percent Anorthite). The average composition of typical syenites (SY) is shown by the large red circle and was deterined by Le Maitre (1976). Note how far removed SY is from the compositions of syenites compiled by Morse et al. (2007).

As can be seen in this figure, Morse et al. (2007) plotted the average composition of known syenites to have an Mg# greater than 40 and to have feldspars more towards the Na end-member (albite) than the Ca end-member (anorthite) of the plagioclase solid solution series. According to Bowen's Reaction Series, however, this would mean that

the mafic minerals (olivines and pyroxenes) have evolved to a lesser degree than the feldspars (anorthite and albite) of the same rock (Morse et al., 2007).

Although compositional variations exist within the collection of known syenites, one constant among syenites seems to be this presence of feldspars that have been more compositionally evolved towards the Na-rich albite member (Figure 4). The variation of Mg within mafic components of the system seems to play an important role in feldspar composition. As shown in Figure 5, increasing Mg pushes the cotectic of the Olivine-Albite-Anorthite system down towards feldspars that melt at a lower temperature (Morse et al., 2007). Therefore, unlike the path of igneous rock evolution portrayed by Bowen's Reaction Series, previous studies on syenites have shown a trend towards more compositionally-evolved feldspars in the same system with more primitive mafic components that are richer in Mg. Once again, this would lead to the conclusion that the feldspars have traveled further along their compositional evolution than the Mg-rich mafics (Morse et al., 2007). Of particular interest, therefore, is further determination of the relationship between Mg# and An-content of plagioclase.

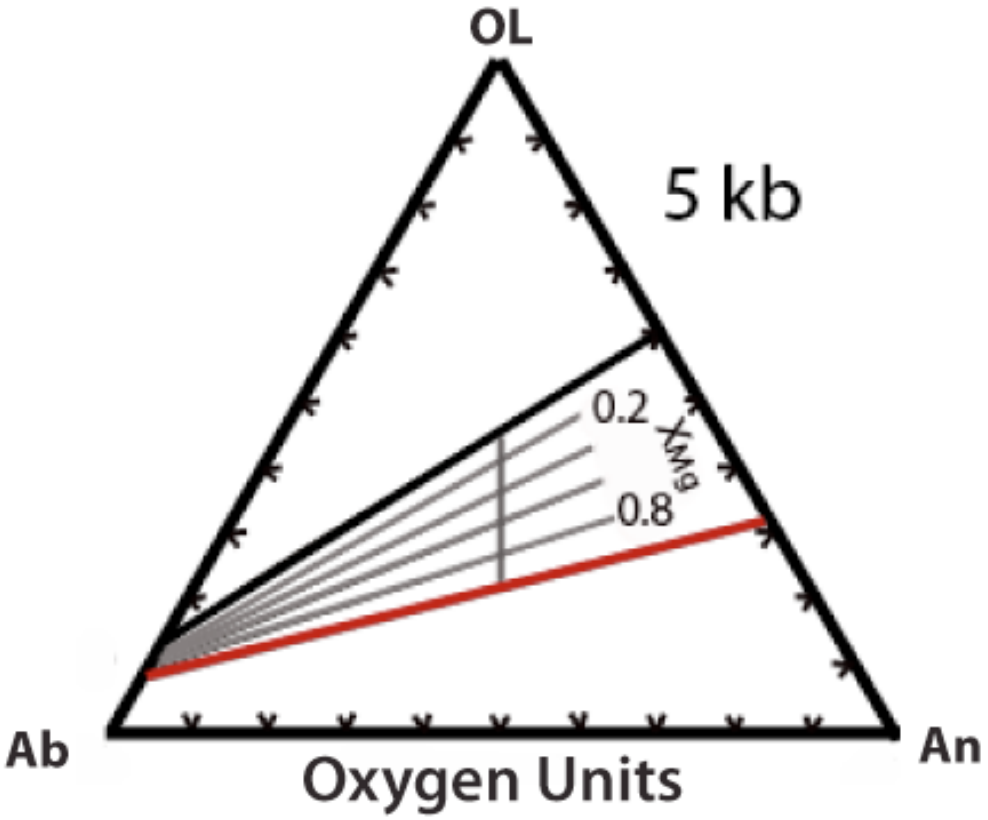

Figure 5. Ternary phase diagram of olivine, anorthite, and albite hypothesizing the relationship between Mg# and An-content of plagioclase based on limited data for the Fa-An-Ab system. The top diagonal line (closest to olivine corner) is the Fo-An-Ab cotectic while the bottom, grey diagonal line represents the Fa-An-Ab cotectic. Figure from (Morse et al., proposal, 2007)

Objectives

The overarching goal of this study is to determine more precisely the cotectic locations of the Fo-An-Ab system by simulating the compositions of various Mg-rich parent magmas at 5 kb pressure. Specific feldspar compositions were mixed and ground with measured proportions of the Mg-rich olivine end member synthetic forsterite (see section on starting materials). Three natural feldspar compositions were used, all

provided by Dr. Tony Morse at the University of Massachusetts Amherst: Na-exchanged Amelia albite from a pegmatite near Amelia Courthouse, Virginia and two mineral separates from the Kiglapait intrusion in Labrador: An_{48} composition and An_{66} composition. Melting temperatures for each mixture were predicted using an equilibrium ternary diagram (Figure 6) for the Fo-An-Ab system with isotherms and cotectic experimentally determined by Schairer and Yoder (1967) at 1 atmosphere pressure. Also of considerable importance was Figure 7 relating the melting behavior of plagioclase feldspar at 1 atm (Schairer and Yoder, 1967), 10 kb, and 20 kb (Lindsley, 1967) as this provided extra assistance in understanding the possible changes that may occur when taking the Fo-An-Ab system from 1 atm to 5 kb pressure.

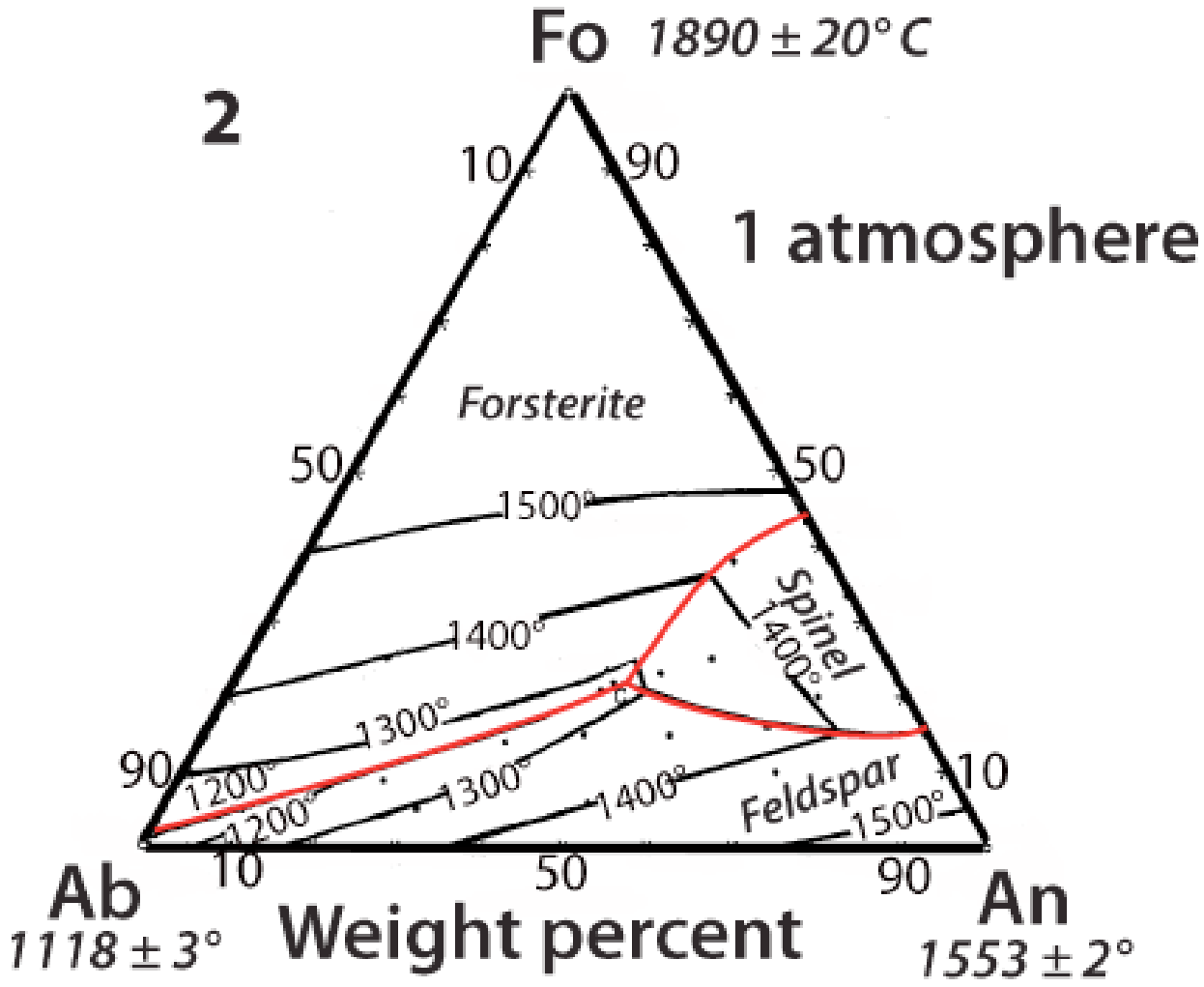

Figure 6. Experimentally determined equilibrium diagram with isotherms and cotectic for the Fo-Ab-An system at 1 atmosphere pressure (Schairer and Yoder, 1967).

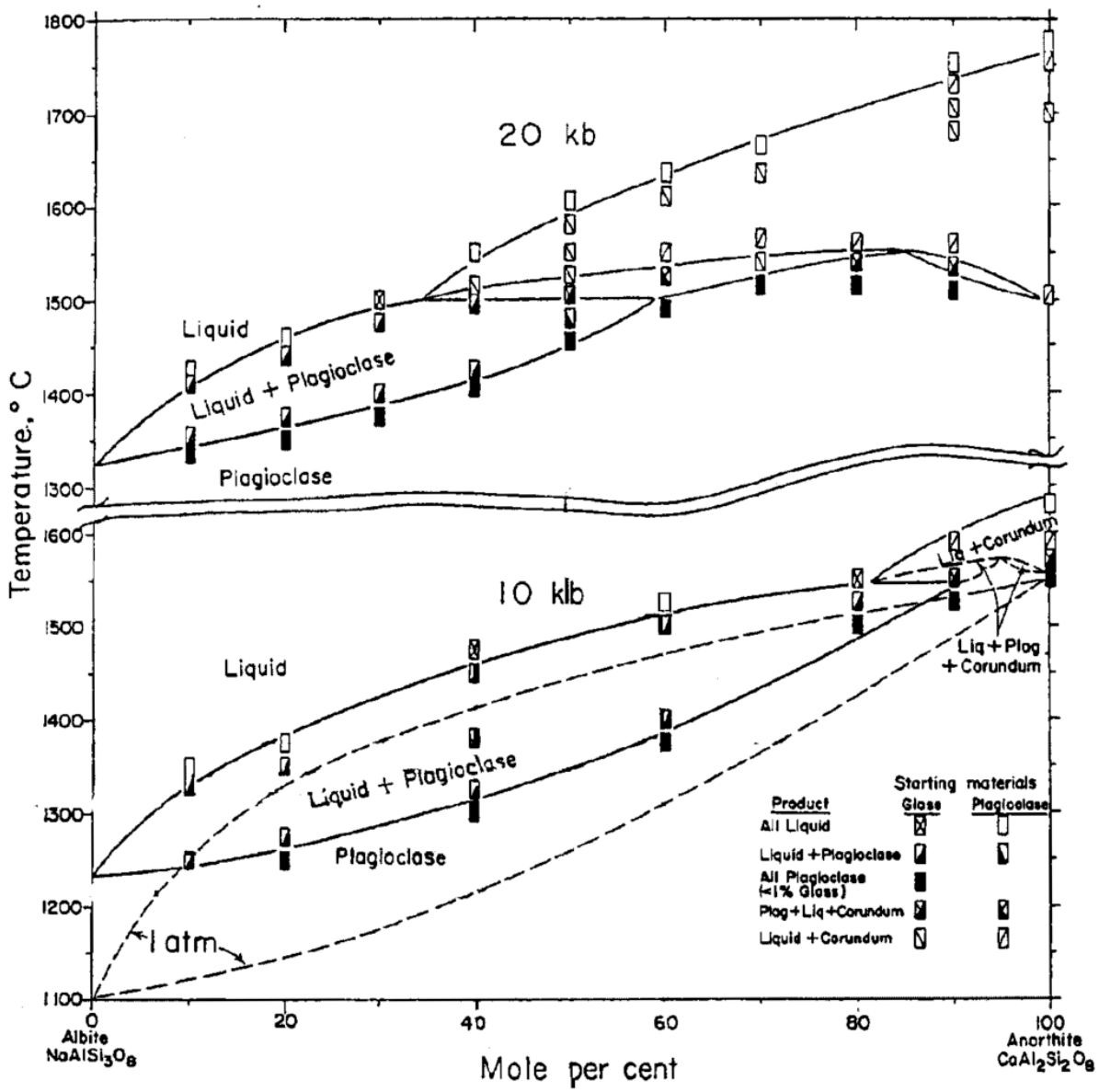

Figure 7. Binary equilibrium lines for the two plagioclase end members albite and anorthite. Compositions of glasses and the crystallized plagioclase are shown in key and uncertainties are shown by the height of the composition symbol boxes. The lighter lines connecting starting materials with a corundum component represent

Sources for Starting Materials

An_{66} and An_{48} feldspar compositions: The Kiglapait Intrusion, Labrador

The key question in this proposal had its basis in previous research of the Kiglapait intrusion in Labrador (Morse et al., 2007; Morse et al., 2004; Morse and Ross, 2004). Additionally, two of the three plagioclase feldspars (An_{66} and An_{48}) provided by Dr. Tony Morse at the University of Massachusetts at Amherst were samples from this intrusion. Therefore, it is important to understand the nature of the Kiglapait and how it compares to syenites found within other layered mafic intrusions.

The Kiglapait intrusion is a Precambrian, layered mafic intrusion covering a total area of 560 km^2 (Winter, p. 219, 2001). The Kiglapait intruded into Archean-Proterozoic country rock to the north and anorthosite to the south at a depth of 9 km and a pressure of approximately 2.5 kb (Morse, 1996). An overview of the layering within the Kiglapait is presented by Morse (1996), dividing the intrusion into two main sections: a Lower Zone (LZ), and an Upper Zone (UZ) (Morse, 1996). While the LZ troctolites contain olivine as their only cumulus mafic mineral, UZ rocks are characterized by both cumulus olivine and augite (Morse, 1996). The syenites comprising the UZ are characterized by fayalite, the Mg-poor end member of olivine (Morse et al., 2007).

What makes the Kiglapait an interesting situation is the fact that it is more or less a closed system, meaning that large batches of fresh magma were not introduced (Morse, 1996). Chemical variations exist when comparing the Kiglapait with other layered intrusions. Morse et al. (2007) note that the Kiglapait syenites have a chemical composition that is lacking in Mg compared with typical syenites. For example, syenites within the Bohemia Massif in the Czech Republic are characterized by forsterite, the Mg-

rich end member of olivine (Parat et al., 2009). A constant among syenites, however, is the presence of highly evolved feldspars towards albite and even alkalic compositions (Morse et al., 2007). The two Kiglapait feldspar compositions used in this study were therefore intermediate between the pure albite and pure anorthite compositions at An_{48} and An_{66}. The Kiglapait intrusion does differ from other syenites in that pure albite compositions are not found and more evolved, Mg-free (fayalite) olivine compositions are present (Morse et al., 2004; Morse, 1996). The question, therefore, remains as to how syenites of varied localities and compositions can be connected in terms of their origination and evolution.

Pure Amelia Albite:

For the pure albite composition, NaCl exchanged Amelia Albite was provided by Dr. Tony Morse at the University of Massachusetts at Amherst.

Synthetic Pure Forsterite:

Forsterite used in this study was synthetic boule produced by Union Carbide.

Chapter 3: Experimental Procedure

Perhaps one of the more challenging and rewarding aspects of this project has been the opportunity to learn experimental techniques. Fortunately, the setup and procedures described previously by Morse et al. (2004) could be followed. However, not all experiments are the same and problems that arose had to be resolved with the project at hand in mind.

Powder Preparation

Before each run, a specific feldspar composition was chosen to be mixed with the forsterite. Three different powders were created by carefully weighing out different weight percent feldspar compositions to the forsterite. The three different possible feldspar compositions were Amelia Albite (approximately pure albite composition), An_{66}, and An_{48}, all of which were provided by T. Morse at the University of Massachusetts Amherst. Each feldspar powder was ground further into a finer powder and dehydrated for at least an hour in a 65°C oven. Pure forsterite crystals were crushed and ground into a fine-grained powder and also put in the oven to dehydrate. It was important that each powder be fine-grained in order to ensure homogeneous grain size for melting (Morse et al., 2004).

The compositional mixtures could be made after each powder was sufficiently dehydrated. Three mixtures were made for each run: one that had a greater percentage of feldspar, a second with 60% - 50% feldspar, and the last with a greater percentage of forsterite. Weight percentages were carefully measured in order to put together each

mixture. The total amount of powder was kept constant for each mixture and was typically between 7 mg and 10 mg for each run.

Sample Assembly:

Perhaps one of the most time-consuming aspects of this project was the preparation needed before a run to set up the sample assembly. As shown in Figure 8, each component of the sample assembly had to be made to very specific dimensions in order to ensure proper distribution of pressures and temperatures. Fortunately, some of the assembly pieces were already available for use from previous experiments. The graphite capsules and magnesium oxide (MgO) ceramic spacers all had to be cut to specific lengths so that they fit snugly within the assembly. Additionally, multiple salt sleeves and a thermocouple assembly had to be made for each individual run. One of the challenging aspects of experimental petrology, therefore, is the fact that none of these components can be reused for future runs. In this way, it is of utmost importance that sample assembly be kept consistent throughout experimentation.

In accordance with the recommendations made by Morse et al. (2004), powders were housed in graphite capsules during melting. This kept the oxygen fugacity low during each run, promoting the growth of homogeneous, euhedral crystals (Morse et al., 2004). The capsules were made to be approximately 8 mm in length with three 2 mm wide holes drilled into the top of the capsule for the powders. Each hole was consistent in depth for each mixture in a single run. However, depths varied between 2.5 mm to 8 mm among runs. Hole depths used changed throughout the study as improved experimental techniques were developed. The downfalls and benefits to having a deep versus shallow

hole depth will be explained further when discussing post-run sample preparation techniques. In order to keep clear the location and composition of each powder, a small piece of platinum wire was dropped into the hole of the feldspar-rich mixture. In this way, the orientation of the other two mixtures could be noted in relation to the platinum-bearing hole. The platinum would be apparent in the feldspar-rich hole after polishing. After the three sample mixtures were put into their separate holes, each was packed down and the remaining hole space was filled with graphite powder. Each graphite capsule had an accompanying, less than 1 mm thick graphite lid (Morse et al., 2004). In addition to keeping oxygen fugacity low, graphite is also a useful capsule material as it is inert and also easy to work with (Morse et al., 2004).

Once filled with the three sample mixtures, the graphite capsule and lid were snugly placed in a fired-prophyllite container. The assembled components were then placed in a 45 mm long graphite furnace between two 30 mm length MgO spacers. The top spacer had a 1 mm diameter hole through its center to allow for insertion of the thermocouple.

The graphite furnace was then placed inside a hollow pyrex sleeve which was then inserted into the hollow halite sleeves. Usually two halite sleeves of about 23 cm each were sufficient to envelope the entire length of the pyrex sleeve. In order to better safeguard against the assembly slipping through the sleeves and onto the floor, a small amount of duco cement was used to glue the halite pieces around the pyrex (Figure 6).

At this point a square of lead foil was carefully cut to fit exactly around the diameter of the sample assembly, making sure to not overlap the two foil ends. A small, less than one mm length of lead foil was folded over the bottom of the sample assembly

to ensure easier insertion into the piston-cylinder apparatus. However, a very important part of this step was making sure the lead foil did not come into contact with any part of the pyrex sleeve or graphite furnace. This was to ensure that no current besides that at the contact between thermocouple and graphite capsule would exist.

The final part of the sample assembly, before putting together the thermocouple, was the putting a stainless steel base plug into a fired prophyllite base plug sleeve. The base plug and sleeve were gently dropped onto the top of the sample assembly once in the piston cylinder apparatus.

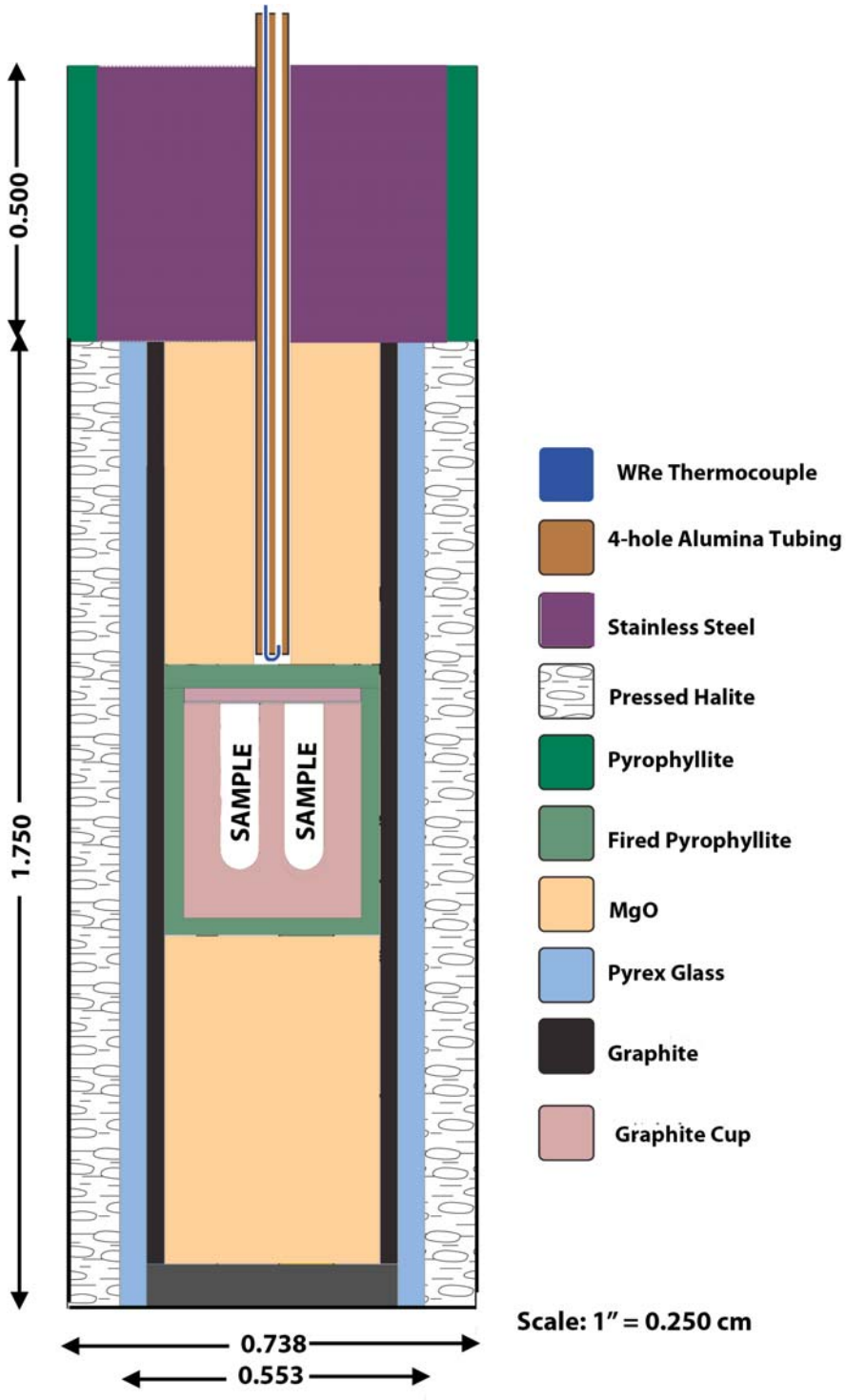

Figure 8. Sample assembly used for all runs.

Thermocouple Assembly:

Preparing the thermocouple assembly was one of the more challenging aspects of the pre-run procedure. As the mechanism through which the temperature of the sample mixtures is read and sent back to the control panel as a voltage, it was of pivotal importance that the thermocouple assembly be carefully constructed. Type D W-Re thermocouple wires were thread through two alumina thermocouple sleeves, together between 2.25 and 2.50 inches in length (Morse et al., 2004). The wires were kept separated until the very tip of the second alumina sleeve where they were crossed and reinserted into the alumina.

Piston Cylinder Apparatus:

The following figure (Figure 9) is a representation of the piston cylinder apparatus setup used for all runs following that used by Morse et al. (2004**).** In order to better simulate the natural setting of syenite formation, a pressure of 5 kb was used for each run. Although syenites can form at pressures less than 5 kb, such as with the emplacement of the Kiglapait intrusion at 2.5 kb, Morse et al. (2004) recommend using 5 kb as pressures lower than this cannot be used with the piston-cylinder design due to uncertainties related to friction.

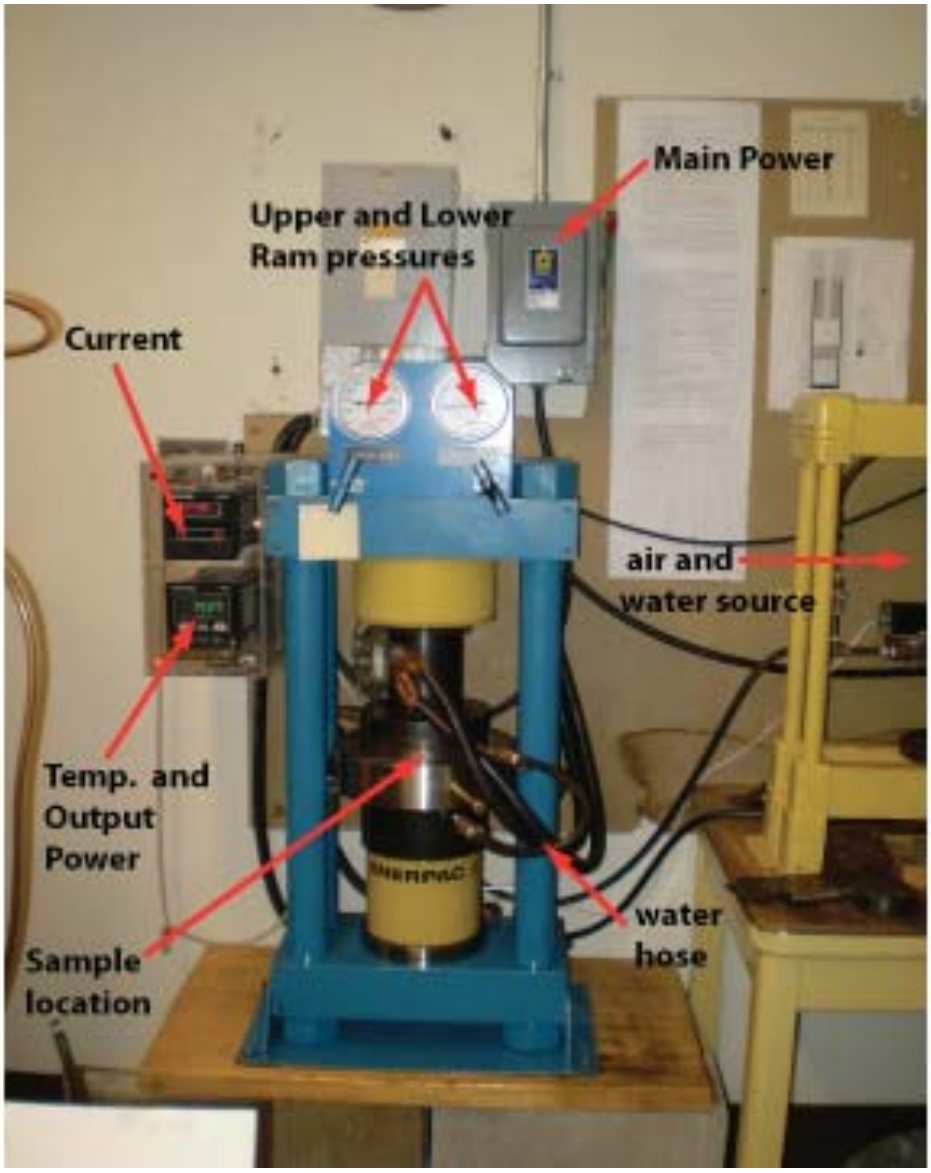

Figure 9. The piston-cylinder apparatus setup used for all runs. The piston-cylinder mimics high pressures and temperatures in order to better understand natural processes occurring at these conditions. Important parts of the apparatus are labeled.

Post-Run Sample Preparation

After completing the run, each sample assembly had to be taken apart so that the graphite capsule could be removed. Once the graphite capsule was freed from the rest of the sample assembly it was mounted in a ring holder with epoxy glue. This made it easier to polish the sample as well as served as a holder for SEM analyses (Figure 10).

Both the graphite lid and the graphite powder had to be ground through in order to reach the sample mixtures. Using a lap wheel, each graphite capsule was ground down to the sample mixtures and then polished. In order to gain a mirror-like polish, the exposed surfaces of each sample mixture was further polished using a 6 micron, 3 micron, and then 1 micron lap wheel. One challenging aspect of the grinding and polishing stage was making sure that one sample mixture was not completely ground away. As mentioned previously, the various powder volumes within each sample hole make this particularly difficult. An additional challenge is the fact that some samples, if ground too far, can even completely fall out of the hole.

The final step before SEM analysis was to carbon coat the sample with a carbon evaporator (Figure 11).

Figure 10**.** Post-run graphite capsules were placed in a sample holder and set in epoxy resin. Weights were used to keep the epoxy within the holder as it hardened.

Figure 11. Image of a sample polished, carbon coated, and ready to go into the SEM for analysis. Actually sample mixtures are the 2 mm diameter darker spots within the graphite capsule.

Chapter 4: Results

Table 1: Run conditions, sample mixture proportions, and calculated percent crystalline and glass amounts

Sample name	Bulk Composition (percent feldspar: fsp)	Percent Crystalline*	Percent Glass*	Final Run Temp (º C)	Run Time (min)
E1	95% Amelia Albite	NE		1130	122
E1	60% Amelia Albite	NE		1130	
E1	20% Amelia Albite	NE		1130	
E2	95% Amelia Albite	NE		1150	248
E2	55% Amelia Albite	NE		1150	
E2	20% Amelia Albite	NE		1150	
E3	95% An_{66}	CEF		1380	127
E3	55% An_{66}	NE		1380	
E3	20% An_{66}	NE		1380	
E4	95% An_{66}	CEF	100%	1340	151
E4	55% An_{66}	44.2% olivine, NE	55.8%	1340	
E5	Current cut out				
E6	95% An_{48}	0.36% (Cl-K)**	99.6%	1300	181
E6	55% An_{48}	48.7% olivine	51.3%	1300	
E6	20% An_{48}	93.6% olivine	6.4%	1300	
E7	95% An_{48}	75.9% feldspar	24.1%	1270	120
E7	60% An_{48}	65.9% olivine	34.1%	1270	
E7	20% An_{48}	23.3% olivine	76.7%	1270	
E8	95% An_{66} – cross section	Slightly plots off bulk composition		1285	128
E9	Samples lost in grinding				
E10	Current cut out				
E11	95% An_{66}	CEF		1270	137
E11	60% An_{66}	NE		1270	
E11	20% An_{66}	NE		1270	
E12	95% An_{66}	CEF		1420	127
E12	20% An_{66}	NE		1420	
E12	20% Amelia Albite	NE		1420	

* Percent crystalline and percent glass calculated using ImageJ software. If the percentages were not examined using ImageJ (mostly due to poor image quality), the possible chemical evidence of crystals is noted with CEF (chemical evidence for feldspar crystals). If the glass composition appears to plot on the bulk composition, NE (no evidence for feldspar crystals) is noted. Compositions with no indication are not far enough from the bulk composition to be certain.

** Strange Cl-K crystals could have effected where this composition plots.

Experiment 7 SEM – BEI (back-scatter electron) image

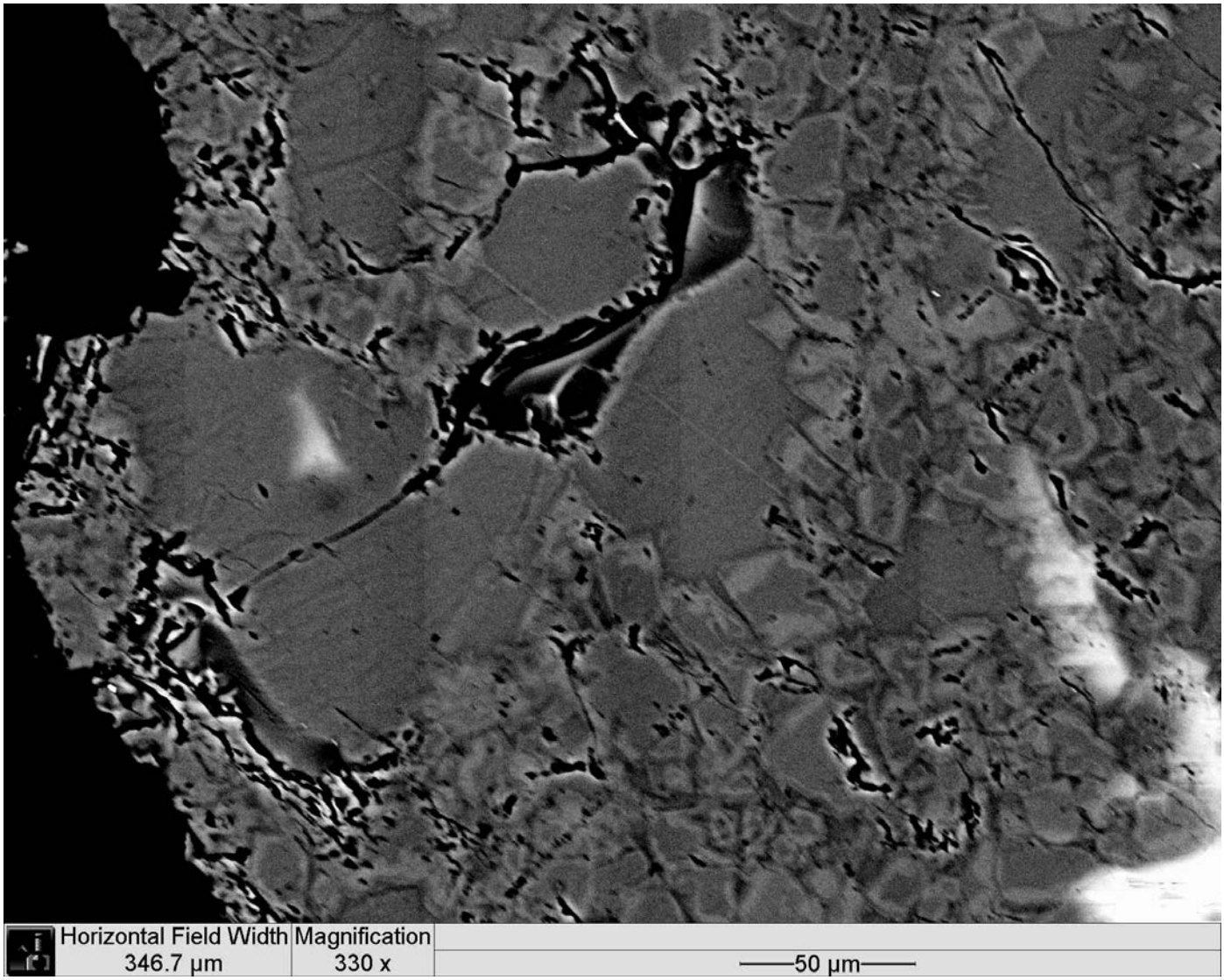

Figure 12. Experiment 7, 95% An_{48} composition. Magnified (330 x) image of feldspar crystals (dark grey – light grey zoned squares) in a glassy matrix (massive, intercumulus medium-grey). Feldspar crystals are zoned from a Ca-rich center to rims with a higher percentage of Na. Bright white color is charging due to deterioration of the carbon coating.

Experiment 1 SEM – BEI (back-scatter electron) image

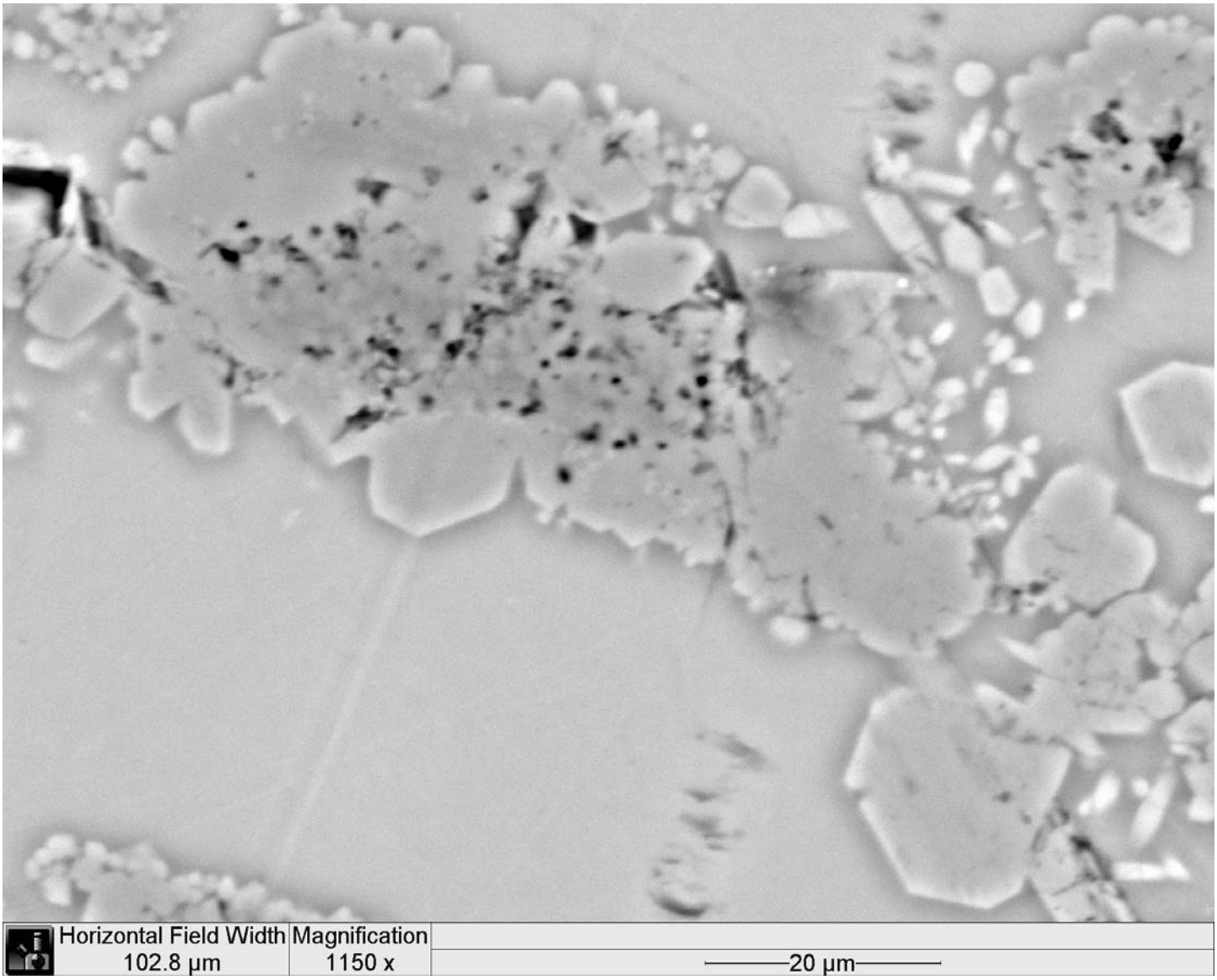

Figure 13. Experiment 1, 20% Amelia Albite (Ab) composition. Olivine crystals (darker grey) in a glassy matrix (lighter grey). White rims on olivine crystals are imaging artifacts related to melt-crystal interactions.

Experiment 4 SEM - BEI image

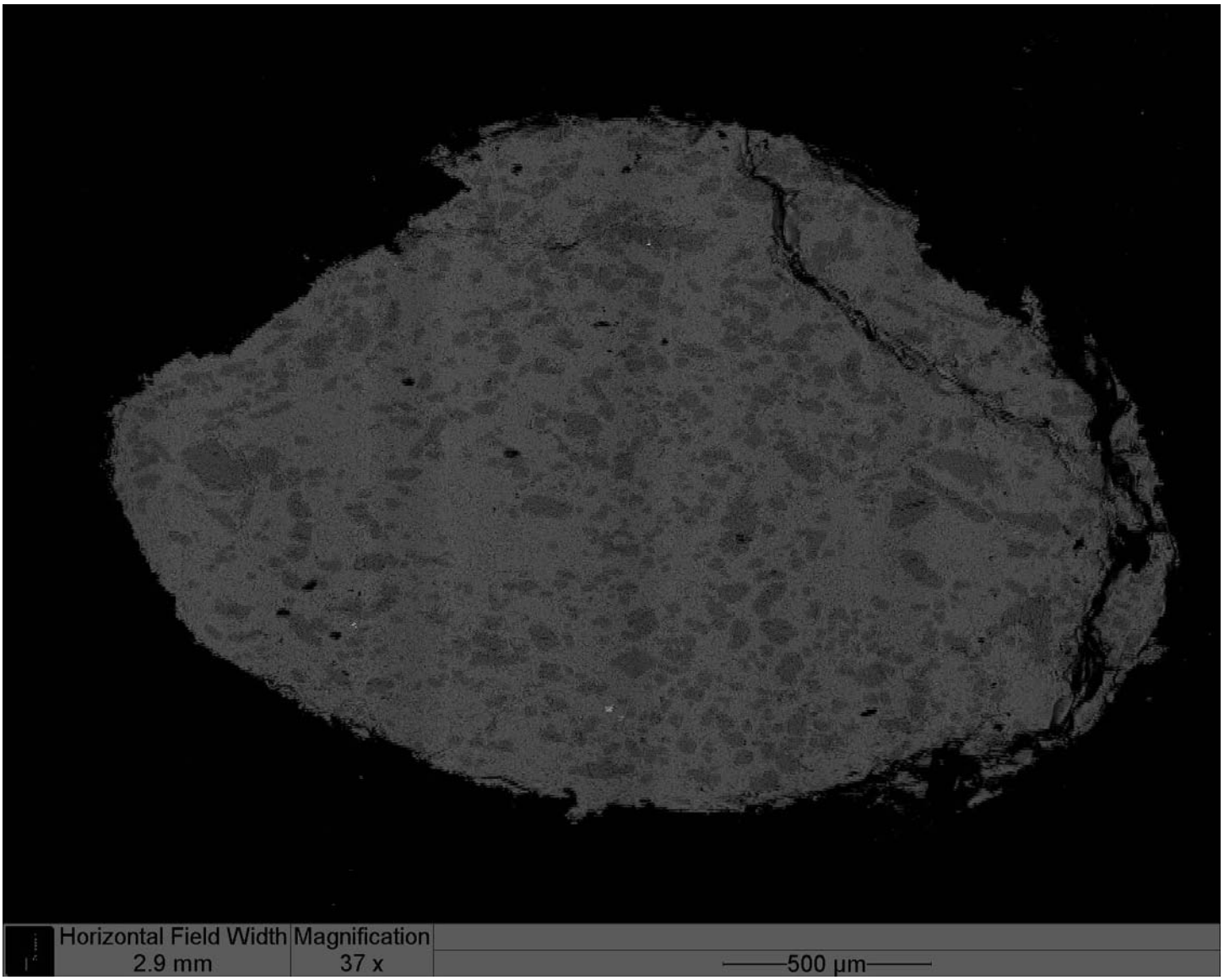

Figure 14. Experiment 4, 55% An_{66} composition. Whole-image sample of olivine crystals (dark grey) in a glassy matrix (lighter grey).

Chapter 5: Discussion

After SEM analyses were completed using the same predetermined set of standards, MgO, CaO, and Na_2O quantities were normalized to 8 oxygen units. Each resulting compositional analysis was plotted on a ternary diagram using a plotting program developed by John Brady. This program relates amount MgO, CaO, and Na_2O, representing the forsterite, anorthite, and albite components respectively, with position within the ternary diagram. Bulk compositions were also calculated based off of the amount of each chemical component in An_{48}, An_{66}, Amelia Albite, and forsterite. In order to get the final bulk compositions in moles, the weight percentages of each sample mixture were calculated using the component amounts previously determined for An_{48}, An_{66}, Amelia Albite, and forsterite in the starting material. Inclusion of bulk compositions within the ternary diagram was important in providing a constraint on where glass compositions of fully, non-differentiated magmas should plot.

A ternary diagram illustrates a composition by relating proportions of each component with relative distance from each vertex, in the case of this study MgO, CaO, and Na_2O. Once plotted, trends can be found in the data points and comparisons can be made with the calculated bulk compositions. An important step towards understanding the system in question is to correlate glass composition data points from runs with similar temperatures. These isotherms provide a useful way to describe the behavior of certain compositions at varying temperature ranges. By examining how isotherm gradients change with increasing or decreasing temperature, it is easier to get an idea of how inter-related temperature and composition are.

Once isotherms are drawn on the ternary plot, a cotectic line can be added. The cotectic is the line along which two minerals are in equilibrium with a liquid (magma), rather than only one. A cotectic is the intersection of two liquidus surfaces (saturation surfaces) (Winter, 2001, p.106). The cotectic line is drawn so that it fits the general trend of the data in the best way possible. Due to both time constraints and limitations imposed by the piston-cylinder apparatus, it was not possible to investigate similar compositions at temperatures above 1420°C. For this reason, isotherms at this high temperature range were predicted based on trends observed at lower temperatures.

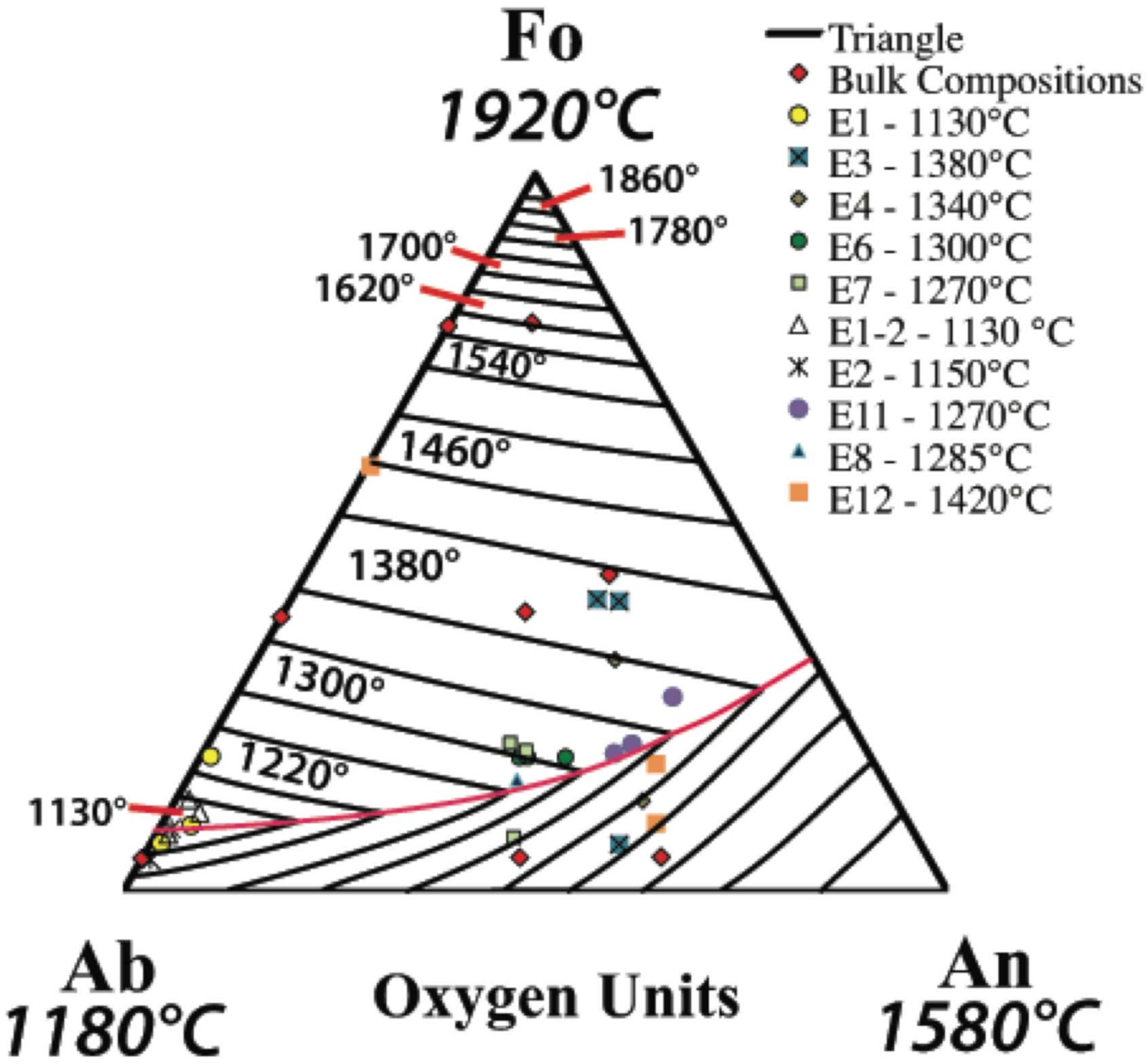

Figure 15. Ternary diagram showing sample compositions plotted from this study along with isotherms (black lines) and a cotectic (red line). All plotted points are glass compositions. The bulk compositions were calculated based on sample mixture proportions (see appendix 2). End-member melting temperatures at 5 kb compiled by Presnall, (1995).

With plotted compositions, isotherms, and a cotectic, a ternary diagram is a useful tool to investigate trends within the Fo-An-Ab system at 5 kb pressure. A basic observation of data points within the ternary diagram derived from this study is that sample mixtures that are seemingly 100% liquid generally plot to the left (towards the Ab vertex) of the corresponding bulk composition. Without crystallization of any kind this would not make sense as the starting composition should be equal to the end composition if no differentiation has occurred. Therefore, it is probable that crystallization actually did occur in these sample mixtures. For example, sample composition 95% An_{48} from Experiment 6 ("E6") at 1300°C appeared to be non-crystalline, made up of 100% glassy material during qualitative SEM analysis. However, as can be seen in Figure 15, its post-run composition was richer in albite than its bulk composition. Drawing a line from the post-run composition and through the bulk composition intersects the An-Ab solid solution axis, providing some evidence for crystallization of Ca-rich crystals. It is by the crystallization of these crystals richer in the An component would have removed the needed Ca from the system to leave the liquid composition with a higher proportion of the albite feldspar component. This would explain the deviation from bulk composition but where were the feldspar crystals?

In order to answer this missing feldspar crystal question, it was important to think of the composition of the system as a whole. A composition such as the 95% An_{48}, 5% Fo proportion of E6 would mean that the melt would be a mixture of Mg, Ca, and Na along with Al and Si. Following Bowen's Reaction Series (Figure 1), the first crystals to form should be richer in Ca (closer to the pure An composition). Shown in Figure 13 is this compositional evolution in the chemically zoned nature of the feldspar crystals from Ca-

rich in the center towards less abundant Ca in the rims. In the periodic table, Ca has a larger atomic weight than Mg, Na, Al, and Si, meaning that the crystals that form will be denser than the melt and should sink to the bottom of the graphite hole. This is why samples that appeared to be 100% glass plotted off of their respective bulk composition: crystals removing Ca from the melt had sunk to the bottom of the graphite hole. Luckily, however, the 95% An_{48} composition from Experiment 7 ("E7") at 1270°C appeared to have been ground down far enough to reach feldspar crystals (Figure 14). The composition of these feldspar crystals was plotted relative to MgO, CaO, and Na_2O as shown on the ternary diagram below (Figure 16). As predicted, the feldspar crystal composition plotted on the An-Ab axis closer to the Ca end-member of plagioclase. This concept of sinking plagioclase crystals is an interesting aspect of working with Mg-rich melts rather than the floating plagioclase crystals found within Fe-rich melts associated with the fayalite end-member of olivine. Unfortunately, physical evidence of these sinking feldspar crystals was not seen in the cross-section cut of the 95% An_{66} composition of Experiment 8 at 1280°C. However, this could have been due to insufficient grinding as the piece of platinum used to identify this composition partly protected the graphite around it from being ground away

Any forsterite crystals that formed, however, were richer in Mg than the Ca and Na-rich melt. These forsterite crystals were more likely to float in relation to the melt, such as is shown by the well-formed olivine crystal from the 20% Amelia Albite composition of Experiment 1 (Figure 12) and the abundant olivine crystals (approximately 44.2% of the sample) from the 55% An_{66} composition of Experiment 4 (Figure 13).

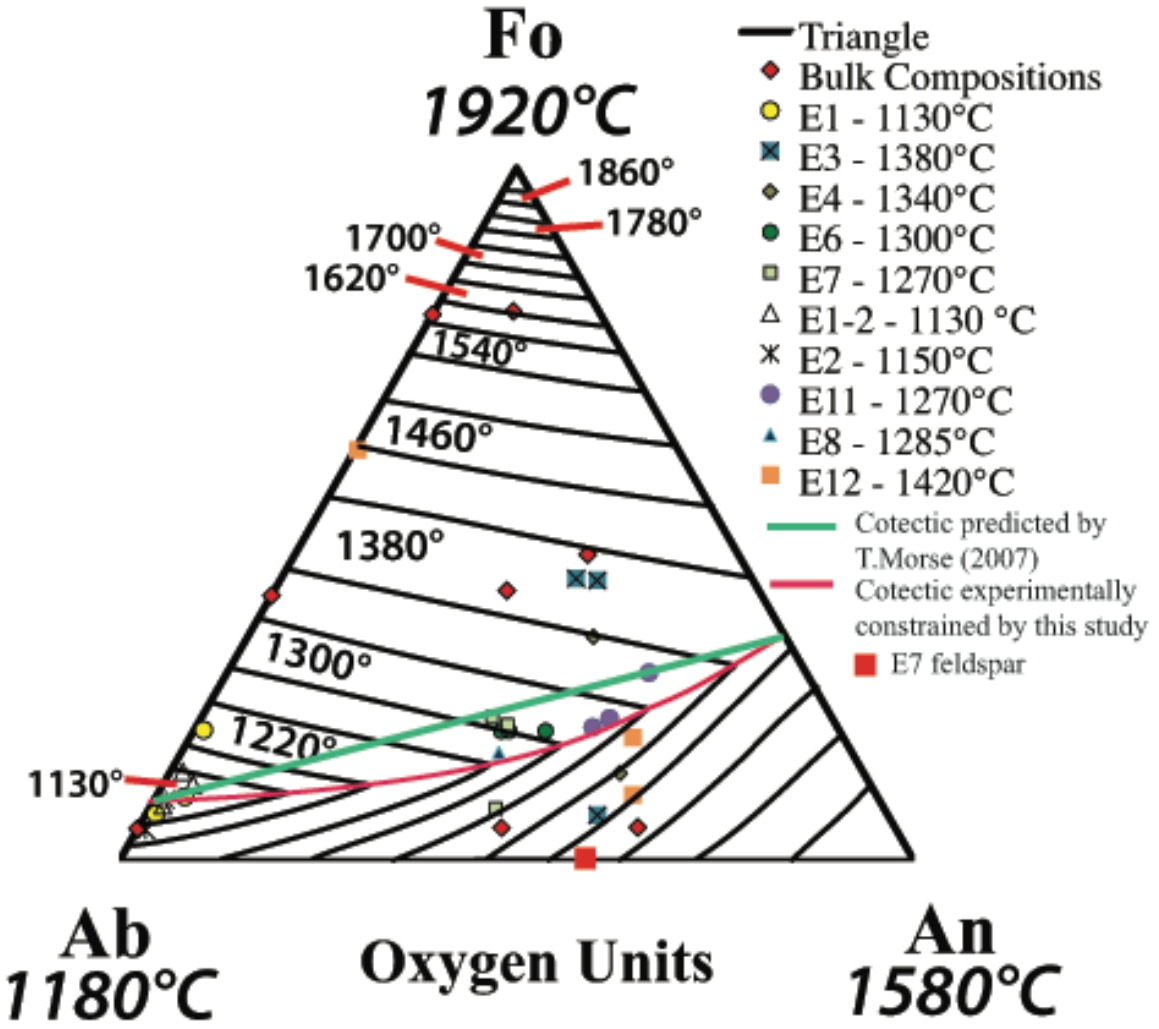

Figure 16. The same ternary diagram as Figure 15 but showing the composition of the feldspar crystals from the 95% An_{48} composition of Experiment 7. End-member melting temperatures at 5 kb compiled by Presnall, (1995).

Another goal of this study was to experimentally constrain what previous researchers have predicted for the location of the Fo-An-Ab system cotectic at 5 kb (Schairer and Yoder, 1967; Lindsley, 1967; Morse et al., 2007).

Some basic observations can be made citing differences between the 1 atm ternary diagram of the Fo-An-Ab system by Schairer and Yoder (1967) and this study (Figure 17). The most obvious of these, as shown by Presnall (1995) in his compilation of major phase diagrams, is an increase in the melting points of each component as per the Gibbs free energy law (Winter, 2001, p. 76). This pressure difference has also excluded the spinel zone that Schairer and Yoder (1967) experimentally found at 1 atm. Due to the higher melting temperature of spinel, an increase in pressure from 1 atm to 5 kb has pushed spinel towards an even higher melting temperature and off of the Fo-An-Ab ternary diagram. In their review of the spinel zone at 1 atm, Schairer and Yoder (1967) further state that spinel will not exist below 1318° ± 3° C. An increase in pressure could have driven the melting point to well over the 1420° C maximum temperature achieved in this study, thereby avoiding the appearance of spinel within the system.

Also absent within the Fo-An-Ab ternary of this study is the corundum field experimentally observed by Lindsley (1967) towards the An-rich feldspar compositions at 10 and 20 kb pressure. Due to the fact that corundum is stable only within igneous rocks at these higher pressures, this study's look at the Fo-An-Ab system at only 5 kb excludes corundum.

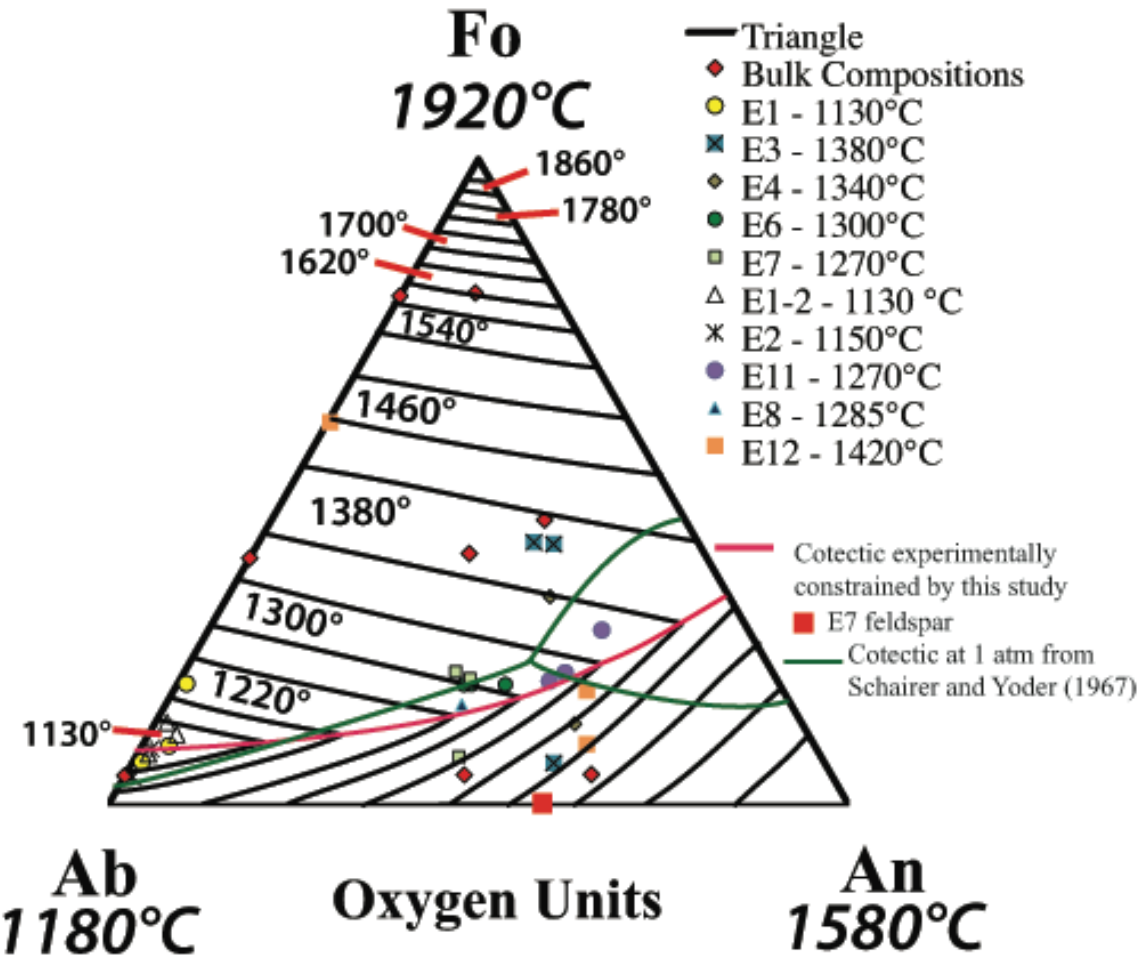

Figure 17. The same ternary diagram as Figure 16 but with the addition of the cotectic from Schairer and Yoder (1967) showing the spinel field present in the Fo-An-Ab system at 1 atm pressure (in weight percent). End-member melting temperatures at 5 kb compiled by Presnall (1995).

Differences in cotectic location also exist between this study and previous studies. Figure 17 is the ternary diagram from this study overlain by the cotectic experimentally determined by Schairer and Yoder (1967) at 1 atm pressure. Due to the fact that the 1 atm cotectic is in weight percent, only qualitative observations can be made between the two cotectics at this point. As can be seen in Figure 17, the location of the cotectic in this study at 5 kb is located further from the pure Ab vertex than that at 1 atm. In terms of crystallization progression, this means that a mixture composition with a larger proportion of Fo relative to Ab is needed in order for both components to exist simultaneously within a system at the melting temperature of pure Ab, or approximately 1180° C.

Also noticeable when comparing the two cotectics is a difference in slope. The cotectic at 1 atm has a greater slope than the cotectic of this study at 5 kb, which only begins to increase in slope towards the An end of the solid-solution series. By using experimentally determined data points, the continuation of the increased slope of the 5 kb cotectic towards the pure An-Fo axis was predicted as shown in the figure.

The general trend of this cotectic line when compared with Figure 5 is consistent with the conclusion of Morse et al. (2007) that increased magnesium content raises the melting range of mafic minerals and will push the cotectic towards the lower-melting feldspar, or Ab in this study. However, the prediction for the location of the Fo-An-Ab cotectic by Morse et al. (2007) underestimated how far the cotectic would actually be pushed towards the feldspar solid solution axis as shown by the cotecic experimentally determined

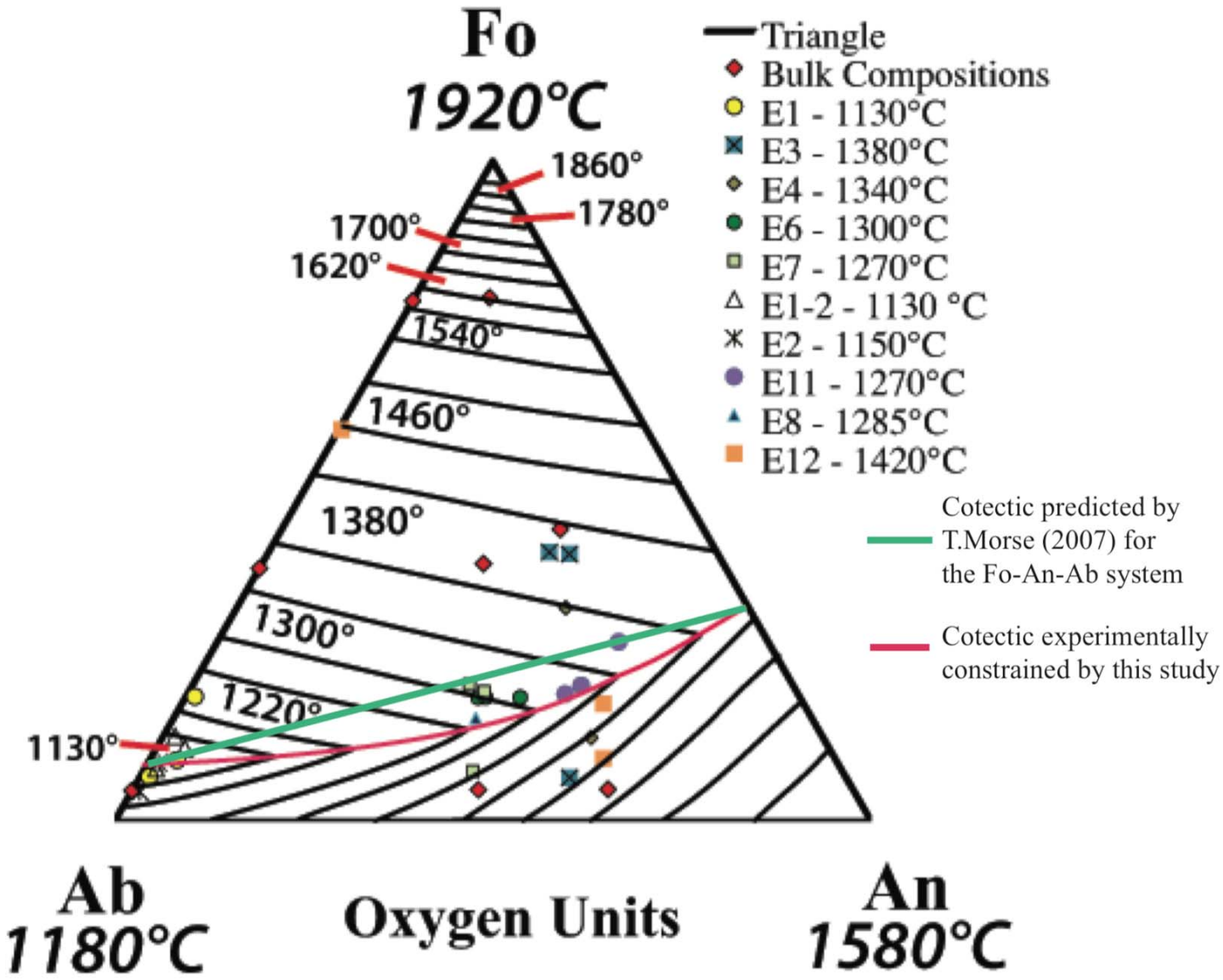

Figure 18. The same ternary diagram as Figure 15 but with the addition of the cotectic predicted for the Fo-An-Ab system by Morse et al. (2007). The location of this cotectic was predicted based off of experimental data from the Fa-An-Ab system. End-member melting temperatures compiled by Presnall (1995).

by this study (Figure 18). By even just comparing the resulting compositions with bulk compositions, it is obvious that the addition of forsterite has a significant role in pushing the cotectic towards the feldspar axis.

An interesting difference between this study's cotectic and that experimentally determined by Morse et al. (2007) for the Fa-An-Ab system is the range over which olivine and plagioclase can coexist in equilibrium. Figure 19 is the ternary phase diagram for the Fo-An-Ab system from this study overlain by the Fa-An-Ab cotectic from Morse et al. (2007), both experimentally investigated at 5 kb pressure. This figure is a helpful representation of how plagioclase composition is related to olivine composition, The isotherm lines determined in this study clearly cannot be correlated to the Fa-An-Ab system. While the Fa-An-Ab cotectic at 5 kb exists over a temperature range of about 27° C, the Fo-An-Ab cotectic exists over a much wider range of approximately 250° C. The reason for this lies in the gradients of the isotherm tie lines. Although not included, the isotherm tie lines for Fa-An-Ab must have had a much smaller overall gradient (Morse et al., 2007). Fayalite has a lower melting temperature at 5 kb than forsterite, making it possible for the isotherms at the top of the ternary diagram to be more spread out. Additionally, isotherms throughout the feldspar equilibrium region would also be further apart than those in this study's diagram due to the larger slope of the cotectic towards the An-Fa join. Once again, this provides support to the hypothesis that Mg will push the cotectic towards the feldspar join, resulting in a steeper temperature gradient towards the pure An and pure Ab vertices (Morse et al., 2007).

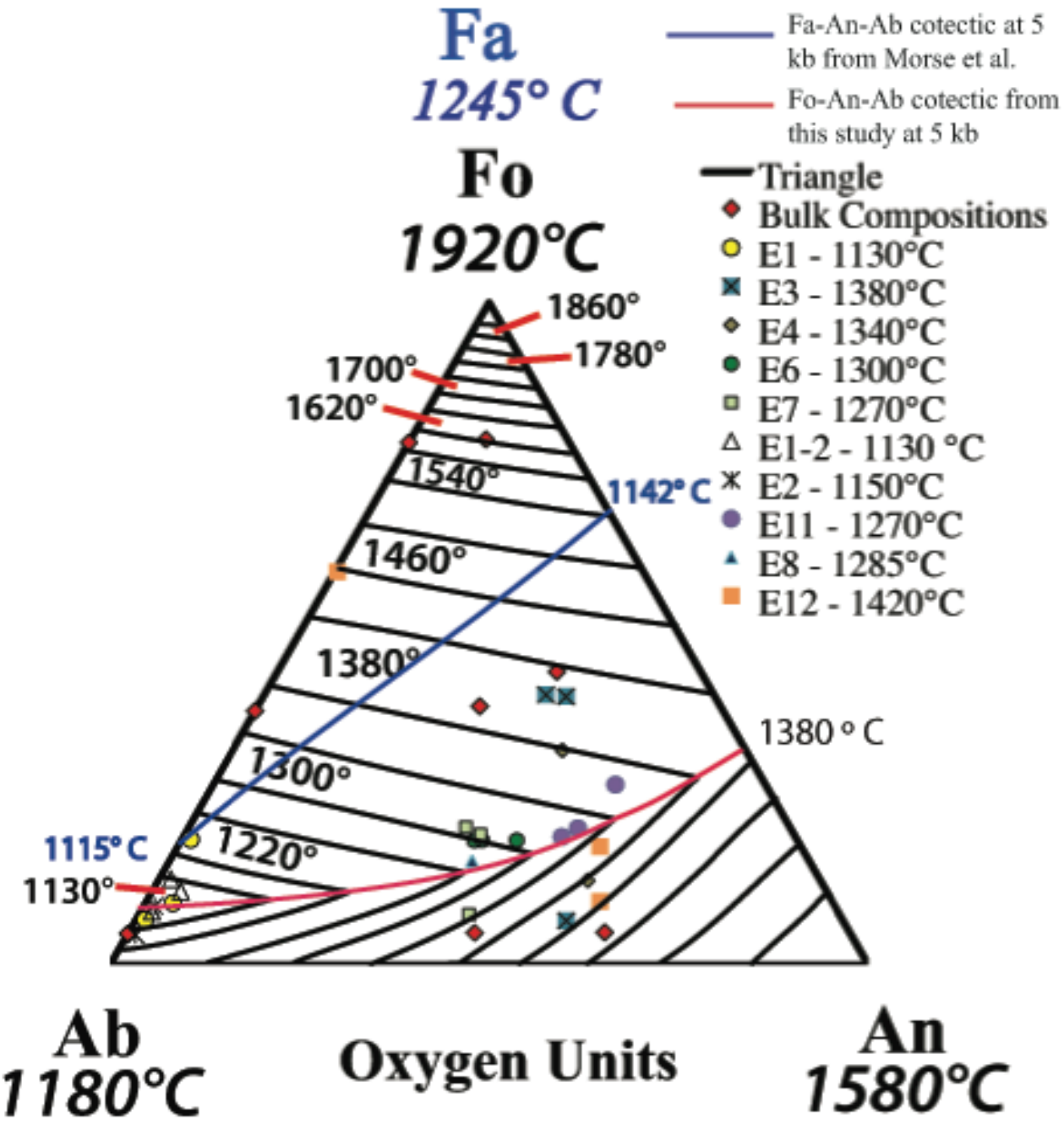

Figure 19. The same ternary diagram as Figure 15 but showing the cotectic Fa-An-Ab experimentally determined by Morse et al. (2007). Note the difference between the temperature range for the Fa-An-Ab (1115ºC - 1142ºC) and Fo-An-Ab (1130ºC - 1380ºC) systems. End-member melting temperatures compiled by Presnall (1995). Fayalite melting temperature from Morse et al. (2007).

Chapter 6: Conclusions

The goal of this study was to constrain the Forsterite-Anorthite-Albite system cotectic at 5 kb pressure by experimentally investigating how the Mg content of olivine affects feldspar compositions. Analyses of the 24 experimentally produced compositions from this study can be compared to data from previous studies in order to understand how the cotectic varies among a variety of mafic compositions, run temperatures, and pressures.

The majority of chemical analyses plotted in this study were of glass compositions. The crystallization of Ca-rich feldspar crystals was not physically seen in most samples due to the effects of density settling. However, chemical evidence of these crystals was found in glass compositions that plotted closer to the Albite vertex than the expected bulk composition. Forsterite crystals, however, were prevalent in the majority of intermediate to forsterite-rich compositions due to a floating of less-dense Mg-rich crystals in a Ca and Na-rich melt.

Comparisons with earlier studies show that the Fo-An-Ab system at 5 kb differs from that at 1 atm (Schairer and Yoder, 1967) by raising the cotectic position at the pure albite end of the ternary diagram. This would result in a greater proportion of forsterite relative to albite needed to get equilibrium between forsterite and pure albite. Also, the spinel field described by Schairer and Yoder (1967) at 1 atm was absent from this study's system at 5 kb.

This study proves the assertion that increased Mg content of olivine pushes the cotectic closer to the Anorthite-Albite join. It is clear that the cotectic spans a wider temperature range than that of the Fa-An-Ab system (Morse et al., 2007). The cotectic

experimentally determined by this study migrates even further towards this feldspar solid-solution axis than previously predicted (Morse et al., 2007).

References Cited:

Bhattacharya, S. and Kar, R., 2005. Petrological and Geochemical Constraints on the Evolution of the Alkaline Complex of Koraput in the Eastern Ghats Granulite Belt, India: *Gondwana Research*, V. 8, No. 4, pp. 596-602.

Blatt, H. and Tracy, R.J., 1996. *Petrology: Igneous, Sedimentary, and Metamorphic*: New York, W.H. Freeman and Company, second edition.

Boyd, F.R. and England, J.L., 1962. Effect of pressure on the melting of diopside and albite: *Journal of Geophysical Research*, V. 67, Issue 9, pp. 3544.

Carmichael, I.S.E., Turner, F.J., and Verhoogen, J., 1974. *Igneous Petrology*: New York, McGraw-Hill Book Company.

Le Maitre, R.W., 1976. The chemical variability of some common igneous rocks: *Journal of Petrology*, V. 17, pp. 589-635.

Lindsley, D.H., 1967. Melting relations of plagioclase at high pressures: *Year Book: Carnegie Institution of Washington*, pp. 204.

Morse, S.A., 1996. Kiglapait mineralogy III; olivine compositions and Rayleigh fractionation models: *Journal of Petrology*, V. 37, Issue 5, pp. 1037 – 1061.

Morse et al., 2007. Origin of syenite and trachyte: a new five-college experimental study. Five-college project proposal.

Morse, S.A., Brady, J.B., and Sporleder, B.A., 2004. Experimental Petrology of the Kiglapait Intrusion: Cotectic Trace for the Lower Zone at 5 kbar in Graphite: *Journal of Petrology*, V. 45, No. 11, pp. 2225-2259.

Morse, S.A. and Ross, M., 2004. Kiglapait mineralogy; IV, The augite series: *American Mineralogist*, V. 89, Issue 10, pp. 1380-1395.

Parat, F., Holtz, F., René, M., and Almeev, R., 2009. Experimental constraints on ultrapotassic magmatism from the Bohemian Massif (durbachite series, Czech Republic): *Contributions to Mineral Petrology*, V. 159, No. 3, pp. 331-347.

Presnall, D.C., 1995. Phase Diagrams of Earth-Forming Minerals: *Mineral Physics and Crystallography: A Handbook of Physical Constants: AGU Reference Shelf 2*, pp. 248 – 268.

Schairer, J.F. and Yoder, H.S., Jr., 1967. The system Albite-Anorthite-Forsterite at 1 atmosphere: *Year Book: Carnegie Institution of Washington*, pp. 204-209.

Winter, J.D., 2001. *An Introduction to Igneous and Metamorphic Petrology*: Upper Saddle River, New Jersey, Prentice Hall.

Appendix 1: Additional Run Information

Experiment 1 – Piston cylinder run: 11/24/2009

Starting materials: Amelia Albite; powdered, pre-bottled forsterite

Starting compositions – Proportions by weight percent: 10 mg total powder

1. 95% Ab; 5% Fo
2. 20% Ab; 80% Fo
3. 60% Ab; 40% Fo

Piston cylinder program:

1130°C ± 5°C = target temperature

0°C → 1080°C → 1120°C → **1130°C *** Target temperature reached in 12 minutes

Piston cylinder run:

Time	% Output Power	Degree C	Lower Ram Pressure	Upper Ram Pressure
16:18	19.0	100	1640	8900
	27.8	200		
	33.4	300		
	38.1	400		
	42.1	500		
	46.0	600		
	62.0	900		
	67.5	1000		
16:30	**72.1**	**1130**	**1640**	**8900**
17:50	73.7	1130	1640	8900
18:13	73.2	1130	1640	8900
18:31	73.4	1130	1630	8910
18:32	QUENCH	Drop 500°C in 11 sec.		

Total run time from when stabilized at 1130°C: 122 minutes

***** all temperature plateaus were 10 seconds long for all runs unless otherwise noted.

<u>Experiment 2</u> – Piston cylinder run: 12/18/2009

Starting materials: Amelia Albite; powdered, pre-bottled forsterite

Starting compositions – Proportions by weight percent: 7.75 mg total powder

1. 95% Ab; 5% Fo
2. 60% Ab; 40% Fo
3. 20% Ab; 80% Fo

Piston cylinder program:

1150°C ± 5°C = target temperature

0°C → 1300°C → 1350°C → **1150°C** Note: first heated up to 1350°C and held there for approximately 30 minutes then brought immediately down to 1150°C for final run temperature in order to test whether complete melting of all components occurred.

Piston cylinder run:

Time	% Output Power	Degree C	Lower Ram Pressure	Upper Ram Pressure
18:11	18.8	100		
	27.2	200		
	32.4	300		
	36.2	400		
	40.7	500		
	45.2	600		
	50.2	700		
	55.5	800		
	62.2	900		
	68.7	1000		
	74.3	1100		
	80.1	1200		
	82.0	1300		
18:24	83.9	1353		
18:54	83.3	1350		
18:56	81.0	1300		
	75.3	1200		
18:59	74.6	1160		
19:00	74.3	1150		
	80.1	1100*		

Time	% Output Power	Degree C	Lower Ram Pressure	Upper Ram Pressure
19:10		1150		
19:13	74.8	1150	1700	8000
19:31	75.2	1150	1710	8000
19:47	75.0	1150	1700	8000
20:04	74.9	1150	1720	8000
20:20	75.1	1150	1700	8020
20:36	74.6	1150	11730	8020
20:50	74.7	1150	1740	8020
21:10	75.2	1150	1740	8020
21:22	74.7	1150	1710	8020
21:42	75.0	1150	1720	8017
21:58	74.6	1150	1730	8017
22:17	74.7	1150-51	1710	8017
22:32	74.1	1149-50	1700	8020
22:46	74.1	1149-50	1700	8020
23:03	74.2	1149-50	1700	8020
23:16	73.8	1149-50	1700	8020
23:18	QUENCH	Down to 63°C in 1 min.		

***** temperature started to go down unexpectedly, manually raised back up to and held at 1150°C

Total run time from when stabilized at 1150°C: 248 minutes

<u>Experiment 3</u> – Piston cylinder run: 1/15/2010

Starting materials: An_{66} from sample "KI 3645 fsp"; synthetic forsterite boule produced by Union Carbide.

Starting compositions – Proportions by weight percent: 7.0 mg total powder

1. 95% An_{66}; 5% Fo
2. 55% An_{66}; 45% Fo
3. 20% An_{66}; 80% Fo

Piston cylinder program:

1380°C ± 5°C = target temperature

0°C → 1330°C → 1370°C → **1380°C** Target temperature reached in 16 minutes.

Piston cylinder run:

Time	% Output Power	Degree C	Lower Ram Pressure	Upper Ram Pressure
15:24	17.1	100	1630	8000
	24.8	200		
	30.8	300		
	35.7	400		
	40.5	500		
	45.7	600		
	51.8	700		
	58.3	800		
	63.8	900		
	69.8	1000		
	75.0	1100		
	80.6	1200		
	84.0	1300		
	86.3	1370		
15:40	**85.5**	**1380**	**1630**	**8400**
15:55	86.8	1380	1635	8200
16:10	88.0	1380	1650	8100
16:25	88.0	1380	1680	8100
16:35	88.0	1380	1680	8100
16:50	87.8	1380-81	1620	8120
17:07	88.7	1380	1620	8130
17:20	88.0	1380	1620	8130

Time	% Output Power	Degree C	Lower Ram Pressure	Upper Ram Pressure
17:33	88.5	1380	1620	8130
17:47	88.3	1380	1620	8120
	QUENCH	Down to 66°C in 1 min.		

Total run time from when stabilized at 1380°C: 127 minutes

<u>Experiment 4</u> – Piston cylinder run: 2/3/2010

Starting materials: An_{66} from sample "KI 3645 fsp"; synthetic forsterite boule produced by Union Carbide.

Starting compositions – Proportions by weight percent: 10.0 mg total powder

1. 95% An_{66}; 5% Fo
2. 55% An_{66}; 45% Fo
3. 20% An_{66}; 80% Fo

Piston cylinder program:

1340°C ± 5°C = target temperature

0°C → 1290°C → 1330°C → **1340°C** Target temperature reached in 16 minutes.

Piston cylinder run:

Time	% Output Power	Degree C	Lower Ram Pressure	Upper Ram Pressure
15:23	16.0	100	1630	8025
		200		
	29.3	300		
	34.5	400		
	38.2	500		
	42.1	600		
	46.1	700		
	50.7	800		
	57.0	900		
	62.0	1000		
	67.0	1100		
	71.2	1200		
	73.3	1290		
	75.8	1330		
15:37	**75.0**	**1340-42**	**1680**	**8500**
15:44	72.2	1340-41	1650	8080
15:59	73.5	1339-40	1650	8200
16:14	73.5	1339-40	1650	8300
16:32	75.1	1340	1650	8350
16:46	75.1	1340	1650	8400
17:07	75.1	1340	1650	8400
17:22	76.1	1340-43	1680	8100

Time	% Output Power	Degree C	Lower Ram Pressure	Upper Ram Pressure
17:40	75.7	1340	1630	8100
17:58	75.7	1340	1680	8100
18:08	QUENCH	Down to 56°C in 1.5 min.		

Total run time from when stabilized at 1340°C: 151 minutes

Experiment 6 – Piston cylinder run: 2/15/2010

Starting materials: An_{48} from sample "KI 3369 fsp"; synthetic forsterite boule produced by Union Carbide.

Starting compositions – Proportions by weight percent: 10.0 mg total powder

1. 95% An_{48}; 5% Fo
2. 55% An_{48}; 45% Fo
3. 20% An_{48}; 80% Fo

Piston cylinder program:

1300°C ± 5°C = target temperature

0°C → 1250°C → 1290°C → **1300°C** Target temperature reached in 13 minutes.

Piston cylinder run:

Time	% Output Power	Degree C	Lower Ram Pressure	Upper Ram Pressure
10:25		100	1630	8025
	23.5	200		
	28.6	300		
	32.9	400		
	37.1	500		
	40.3	600		
	44.2	700		
	48.2	800		
	52.1	900		
	56.9	1000		
	62.5	1100		
	68.0	1200		
	68.7	1250		
	70.7	1290		
10:38	**70.9**	**1300**	**1650**	**8300**
10:56	71.3	1300	1650	8500
11:00	72.6	1300	1650	8550
11:15	73.2	1299-01	1650	8250
11:30	73.4	1299-00	1680	8050
11:47	73.5	1300	1680	8020
12:00	73.5	1299-00	1680	8250
12:15	73.5	1299-01	1680	8250

Time	% Output Power	Degree C	Lower Ram Pressure	Upper Ram Pressure
13:00	73.6	1300	1680	8250
13:18	73.3	1299-01	1680	8250
13:38	73.2	1299-00	1680	8250
13:39	QUENCH	Down to 60°C in 1.5 min.		

Total run time from when stabilized at 1300°C: 181 minutes

<u>Experiment 7</u> – Piston cylinder run: 2/16/2010

Starting materials: An_{48} from sample "KI 3369 fsp"; synthetic forsterite boule produced by Union Carbide.

Starting compositions – Proportions by weight percent: 10.0 mg total powder

1. 95% An_{48}; 5% Fo
2. 60% An_{48}; 40% Fo
3. 20% An_{48}; 80% Fo

Piston cylinder program:

1270°C ± 5°C = target temperature
0°C → 1220°C → 1260°C → **1270°C** Target temperature reached in 15 minutes.

Piston cylinder run:

Time	% Output Power	Degree C	Lower Ram Pressure	Upper Ram Pressure
13:28	14.8	100		
	23.1	200		
	27.9	300		
	32.6	400		
	36.5	500		
	40.1	600		
	43.3	700		
	46.7	800		
	51.3	900		
	55.8	1000		
	61.1	1100		
	65.5	1200		
	65.0	1220		
	66.5	1260		
13:43	**67.0**	**1270**	**1630**	**8450**
13:56	66.6	1269-71	1630	8500
14:14	66.7	1270	1620	8600
14:30	66.7	1270	1620	8650
14:47	67.3	1270	1650	8400
15:06	67.2	1270	1680	8200
15:26	67.4	1270	1680	8150
15:43	QUENCH	1270		

Total run time from when stabilized at 1270°C: 120 minutes

<u>Experiment 8</u> – Piston cylinder run: 3/6/2010

Starting materials: An_{48} from sample "KI 3369 fsp"; synthetic forsterite boule produced by Union Carbide.

Starting compositions – Proportions by weight percent: 10.0 mg total powder

1. 90% An_{48}; 10% Fo
2. 50% An_{48}; 50% Fo
3. 30% An_{48}; 70% Fo

Piston cylinder program:

1285°C ± 5°C = target temperature
0°C → 1235°C → 1275°C → **1285°C** Target temperature reached in 15 minutes.

Piston cylinder run:

Time	% Output Power	Degree C	Lower Ram Pressure	Upper Ram Pressure
15:37		100	1631	8100
	23.2	200		
	28.9	300		
	33.3	400		
	37.1	500		
	40.7	600		
	44.1	700		
	48.3	800		
	53.0	900		
	58.0	1000		
	63.2	1100		
	68.2	1200		
	69.0	1235		
	69.7	1275		
15:52	**70.5**	**1285**		
16:08	70.4	1284-86	1700	8400
16:23	72.1	1285	1630	8400
16:37	72.0	1285	1630	8500
16:50	71.6	1285	1630	8500
17:05	73.4	1285	1630	8500
17:22	72.5	1284	1630	8500
17:37	73.2	1284	1630	8550

Time	% Output Power	Degree C	Lower Ram Pressure	Upper Ram Pressure
17:52	72.6	1285	1630	8550
18:00	QUENCH	Down to 66°C in 1 min.	1630	

Total run time from when stabilized at 1285°C: 128 minutes

<u>Experiment 11</u> – Piston cylinder run: 3/31/2010

Starting materials: An_{66} from sample "KI 3645 fsp"; synthetic forsterite boule produced by Union Carbide.

Starting compositions – Proportions by weight percent: 10.0 mg total powder

4. 95% An_{66}; 5% Fo
5. 60% An_{66}; 40% Fo
6. 20% An_{66}; 80% Fo

Piston cylinder program:

1270°C ± 5°C = target temperature
0°C → 1220°C → 1260°C → **1270°C** Target temperature reached in 15 minutes.

Piston cylinder run:

Time	% Output Power	Degree C	Lower Ram Pressure	Upper Ram Pressure
10:45	15.5	100	1630	8100
	23.3	200		
	28.4	300		
	33.2	400		
	36.9	500		
	40.8	600		
	44.6	700		
	49.1	800		
	54.9	900		
	60.5	1000		
	65.7	1100		
	70.7	1200		
	70.5	1220		
	72.3	1260		
11:00	**72.6**	**1270**	**1700**	**8200**
11:13	72.8	1269-70	1650	8500
11:36	73.2	1270-71	1650	8650
11:51	73.9	1270	1650	8700
12:12	73.7	1270	1650	8720
12:26	75.2	1270	1650	8750
12:42	75.3	1270	1650	8750
12:57	74.7	1270	1650	8800
13:17	74.4	1270	1650	8800
	QUENCH			

Total run time from when stabilized at 1270°C: 137 minutes

<u>Experiment 12</u> – Piston cylinder run: 4/3/2010

Starting materials: An_{66} from sample "KI 3645 fsp"; synthetic forsterite boule produced by Union Carbide; Amelia Albite

Starting compositions – Proportions by weight percent: 8.5 mg total powder

7. 95% An_{66}; 5% Fo
8. 20% An_{66}; 80% Fo
9. 20% Ab; 80% Fo

Piston cylinder program:

1420°C ± 5°C = target temperature
0°C → 1370°C → 1410°C → **1420°C** Target temperature reached in 14 minutes.

Piston cylinder run:

Time	% Output Power	Degree C	Lower Ram Pressure	Upper Ram Pressure
14:50	14.9	100		
	22.8	200	1630	8150
	28.0	300		
	32.4	400		
	36.5	500		
	39.9	600		
	43.4	700		
	47.4	800		
	52.2	900		
	57.4	1000		
	63.2	1100		
	67.8	1200		
	72.9	1300		
	75.5	1370		
	77.2	1400		
	78.9	1410		
15:04	**77.6**	**1420**		**8300**
15:10	77.2	1419-20	1630	8500
15:24	78.5	1420	1630	8600
15:40	79.4	1420	1630	8650
15:55	79.9	1421	1650	8700
14:12	81.9	1420	1650	8700
14:28	82.6	1420	1680	8700
14:48	81.5	1420	1630	8700

Time	% Output Power	Degree C	Lower Ram Pressure	Upper Ram Pressure
17:11	81.7	1420	1600	8700
	QUENCH	Down to 75°C in 1 min.		

Total run time from when stabilized at 1420°C: 127 minutes

Appendix 2: SEM Chemical Analyses of glasses

SEM glass chemical analyses: weight percent oxide

Composition	Run	Temp. °C	SiO_2	Al_2O_3	MgO	CaO	Na_2O	Total
95% Ab	E1	1130	66.22	17.74	3.79	9.87	9.87	97.85
60% Ab	E1	1130	61.44	17.32	11.80	0.26	9.58	100.40
20% Ab	E1	1130	67.98	14.31	5.17	0.70	9.32	97.48
95% Ab	E2	1150	69.30	20.12	2.22	0.20	9.03	100.86
55% Ab	E2	1150	66.24	17.11	4.00	0.23	7.83	95.40
20% Ab	E2	1150						
95% An_{66}	E3	1380	52.15	29.68	3.76	11.26	4.00	100.85
55% An_{66}	E3	1380	47.00	18.55	22.65	7.17	2.36	97.73
95% An_{66}	E4	1340	52.35	27.91	7.82	12.11	3.63	103.82
55% An_{66}	E4	1340	53.26	22.27	20.82	9.73	2.99	109.08
95% An_{48}	E6	1300	53.27	22.65	8.80	7.55	6.95	99.62
55% An_{48}	E6	1300	51.37	22.30	9.81	7.74	6.89	98.38
20% An_{48}	E6	1300	51.28	21.56	10.36	7.44	6.31	97.23
95% An_{48}	E7	1270	56.00	26.54	4.62	9.26	5.74	102.17
60% An_{48}	E7	1270	51.84	21.52	11.38	7.86	4.61	97.21
20% An_{48}	E7	1270	53.59	22.23	12.22	7.50	4.84	100.37
95% An_{66} – cross section	E8	1285	49.01	21.29	8.25	7.33	4.50	90.38
95% An_{66}	E11	1270	54.07	24.62	11.47	10.32	3.52	104.01
60% An_{66}	E11	1270	49.38	21.14	16.20	11.00	2.27	99.99
20% An_{66}	E11	1270	52.11	23.81	11.53	10.01	3.01	100.46
95% An_{66}	E12	1420	49.52	27.15	5.28	11.58	3.28	96.80
20% An_{66}	E12	1420	50.22	24.77	9.56	10.41	2.73	97.70
20% Ab	E12	1420	56.91	10.87	31.07	6.74E-02	4.05	102.98

SEM chemical analyses of glasses: Mg, Na, Ca stoichiometry – 8 oxygen units

Composition	Run	Temp. °C	Na	Mg	Ca
95% Ab	E1	1130	0.61	0.05	0.34
60% Ab	E1	1130	0.80	0.19	0.01
20% Ab	E1	1130	0.87	0.09	0.04
95% Ab	E2	1150	0.94	0.04	0.01
55% Ab	E2	1150	0.90	0.09	0.01
20% Ab	E2	1150			
95% An_{66}	E3	1380	0.37	0.07	0.57
55% An_{66}	E3	1380	0.22	0.41	0.37
95% An_{66}	E4	1340	0.31	0.13	0.57
55% An_{66}	E4	1340	0.24	0.32	0.43
95% An_{48}	E6	1300	0.54	0.13	0.33
55% An_{48}	E6	1300	0.53	0.14	0.33
20% An_{48}	E6	1300	0.51	0.16	0.33
95% An_{48}	E7	1270	0.49	0.08	0.44
60% An_{48}	E7	1270	0.41	0.20	0.39
20% An_{48}	E7	1270	0.43	0.21	0.37
95% An_{66} – cross section	E8	1285	0.44	0.16	0.40
95% An_{66}	E11	1270	0.31	0.19	0.50
60% An_{66}	E11	1270	0.20	0.27	0.53
20% An_{66}	E11	1270	0.28	0.21	0.51
95% An_{66}	E12	1420	0.31	0.09	0.60
20% An_{66}	E12	1420	0.26	0.18	0.56
20% Ab	E12	1420	0.40	0.59	0.00

SEM chemical analyses of glasses – calculated bulk compositions based on mixture proportions

Composition	Na_2O	MgO	CaO
95% Ab	0.95	0.05	0
60% Ab	0.62	0.38	0
55% Ab	0.57	0.43	0
20% Ab	0.21	0.79	0
95% An_{66}	0.32	0.05	0.63
60% An_{66}	0.21	0.39	0.40
55% An_{66}	0.19	0.44	0.39
20% An_{66}	0.07	0.79	0.14
95% An_{48}	0.50	0.05	0.46
60% An_{48}	0.32	0.39	0.29
55% An_{48}	0.29	0.44	0.27
20% An_{48}	0.11	0.79	0.10

Appendix 3: Additional SEM - BEI Images

Experiment 1:

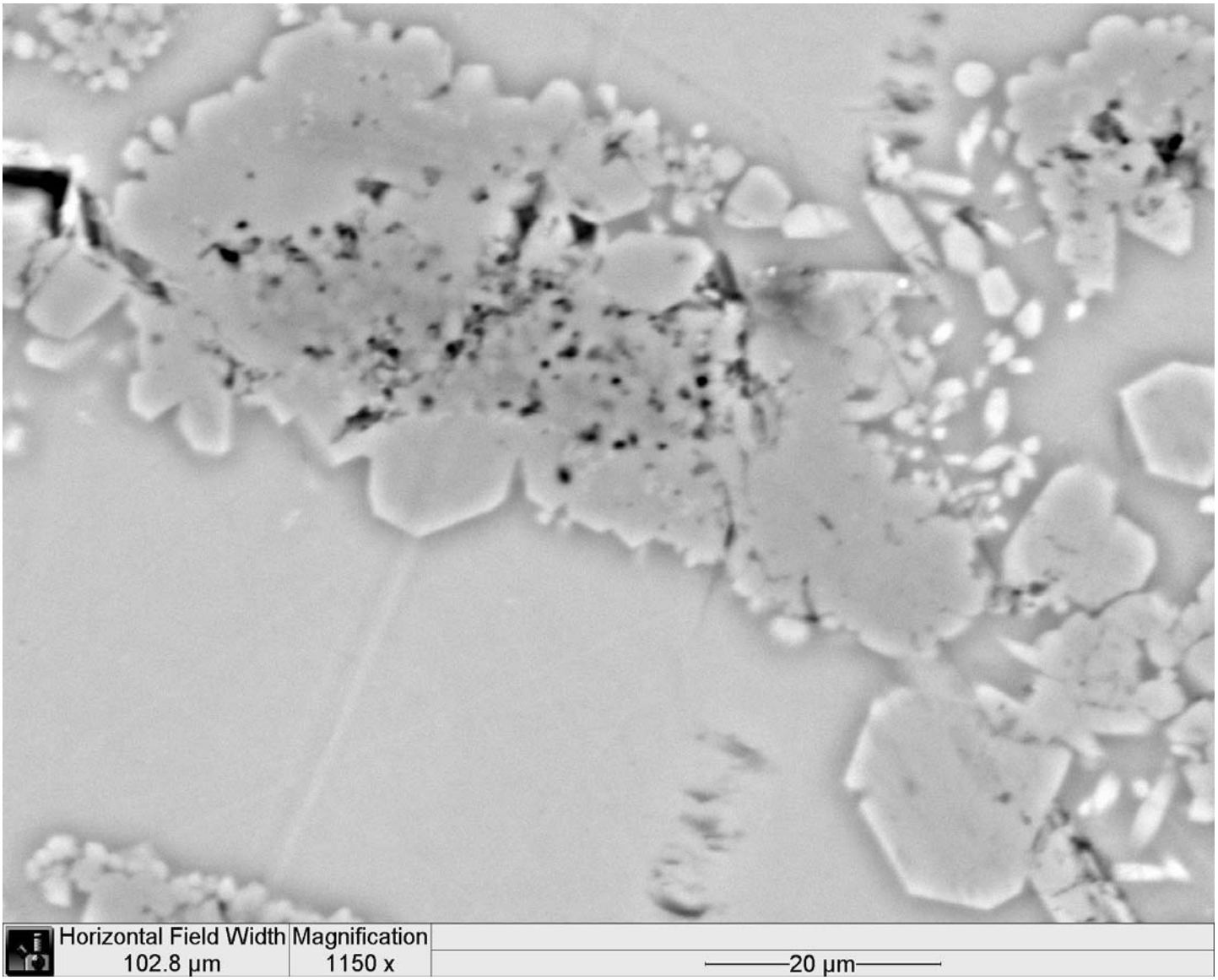

Experiment 1, 20% Amelia Albite (Ab) composition. Olivine crystals (darker grey) in a glassy matrix (lighter grey). White rims on olivine crystals are imaging artifacts related to melt-crystal interactions.

Experiment 4

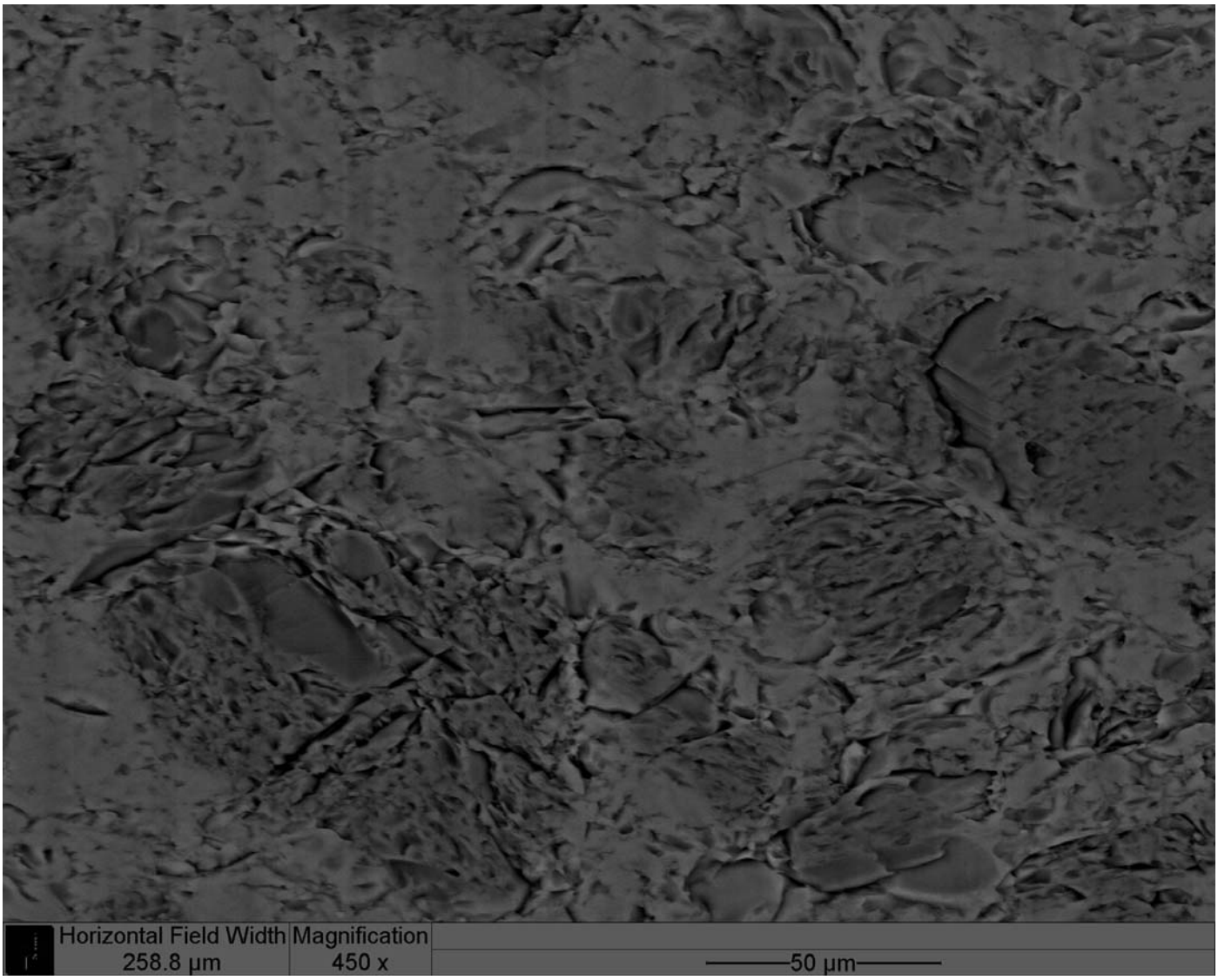

Experiment 4, 55% An_{66} composition. Magnified (450 x) image of olivine crystals (dark grey) in a glassy matrix (light grey). Regardless of sample, olivine crystals showed a characteristic scratched texture from polishing.

Experiment 6

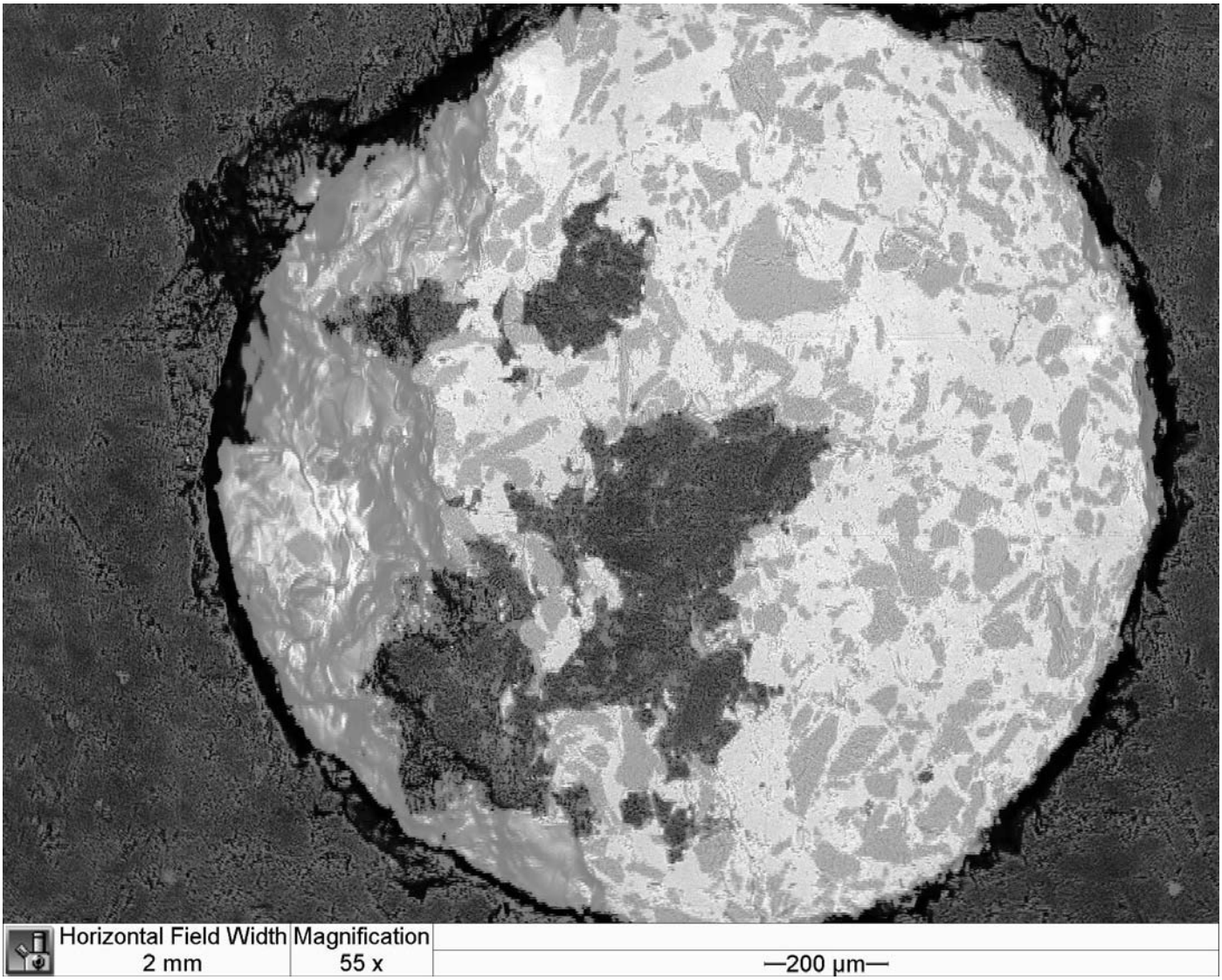

Experiment 6, 55% An_{48} composition.) Whole-sample image of olivine crystals (dark grey) in a glassy matrix (light grey). Topography on left side of sample is due to damage during polishing. Darkest grey material is graphite powder

Experiment 7

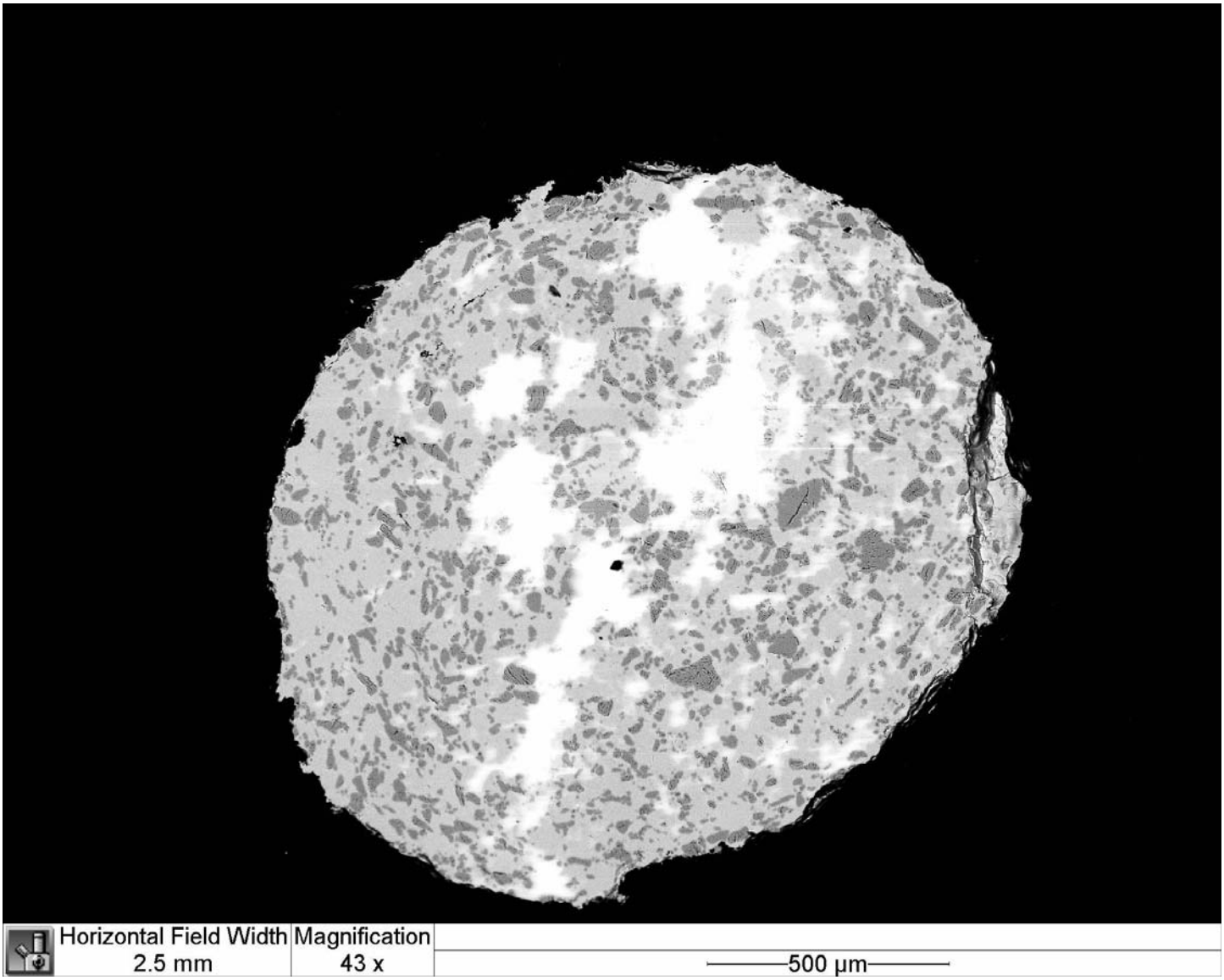

Experiment 7, 60% An_{48} composition. Whole-sample image of olivine crystals (dark grey) in a glassy matrix (light grey). Bright white color is charging due to deterioration of the carbon coating.

Experiment 7

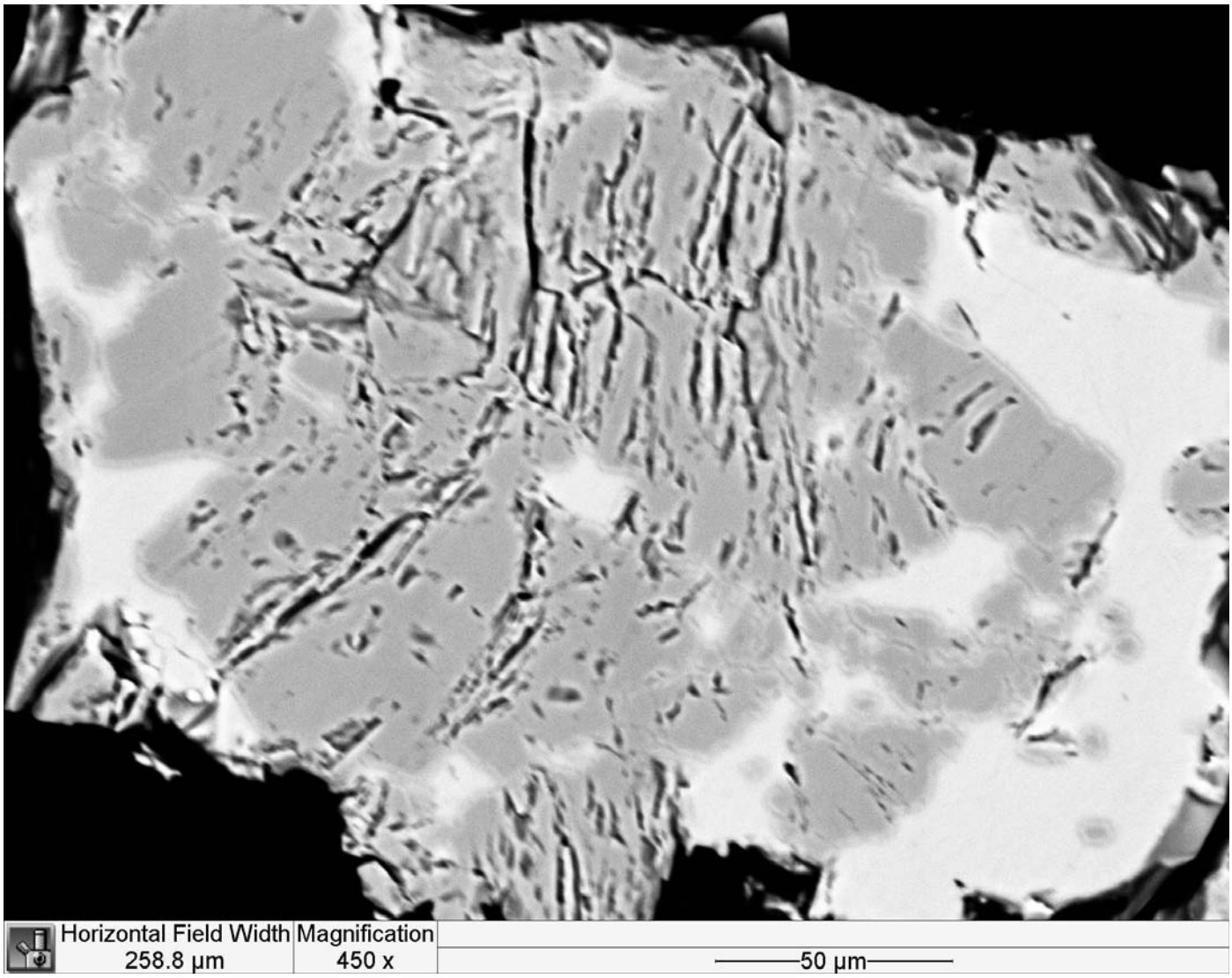

Experiment 7, 20% An_{48} composition. Magnified (450 x) image of the largely crystalline nature of this sample. Olivine crystals (dark grey) are characterized by the left-over polishing topography. Bright white color is charging due to deterioration of the carbon coating.

Experiment 7

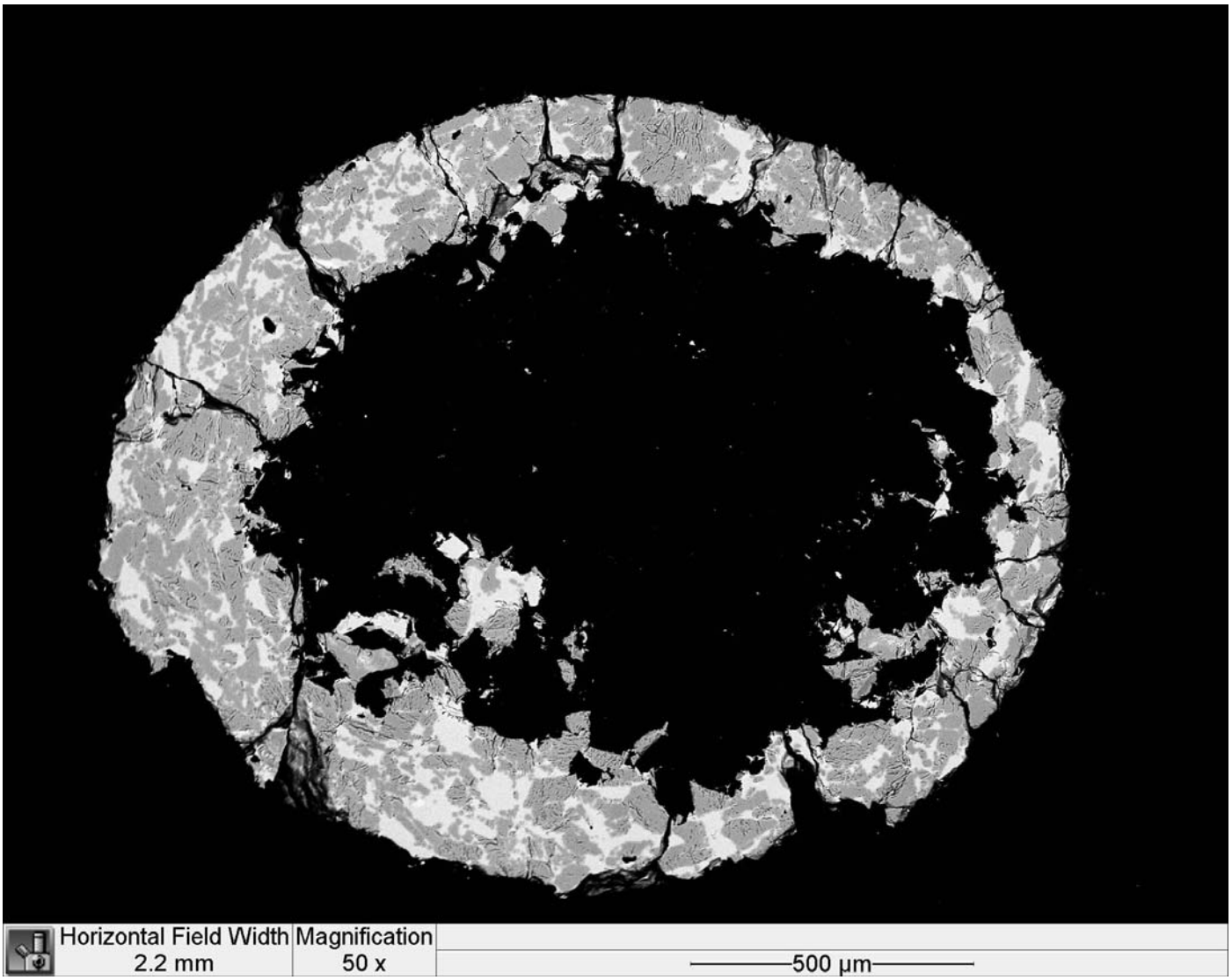

Experiment 7, 20% An_{48} composition. Whole-sample image of the largely crystalline nature of this sample. Olivine crystals (dark grey) are characterized by the left-over polishing topography. Bright white color is charging due to deterioration of the carbon coating. Black material in center of sample is graphite that was not fully ground off.

Experiment 11

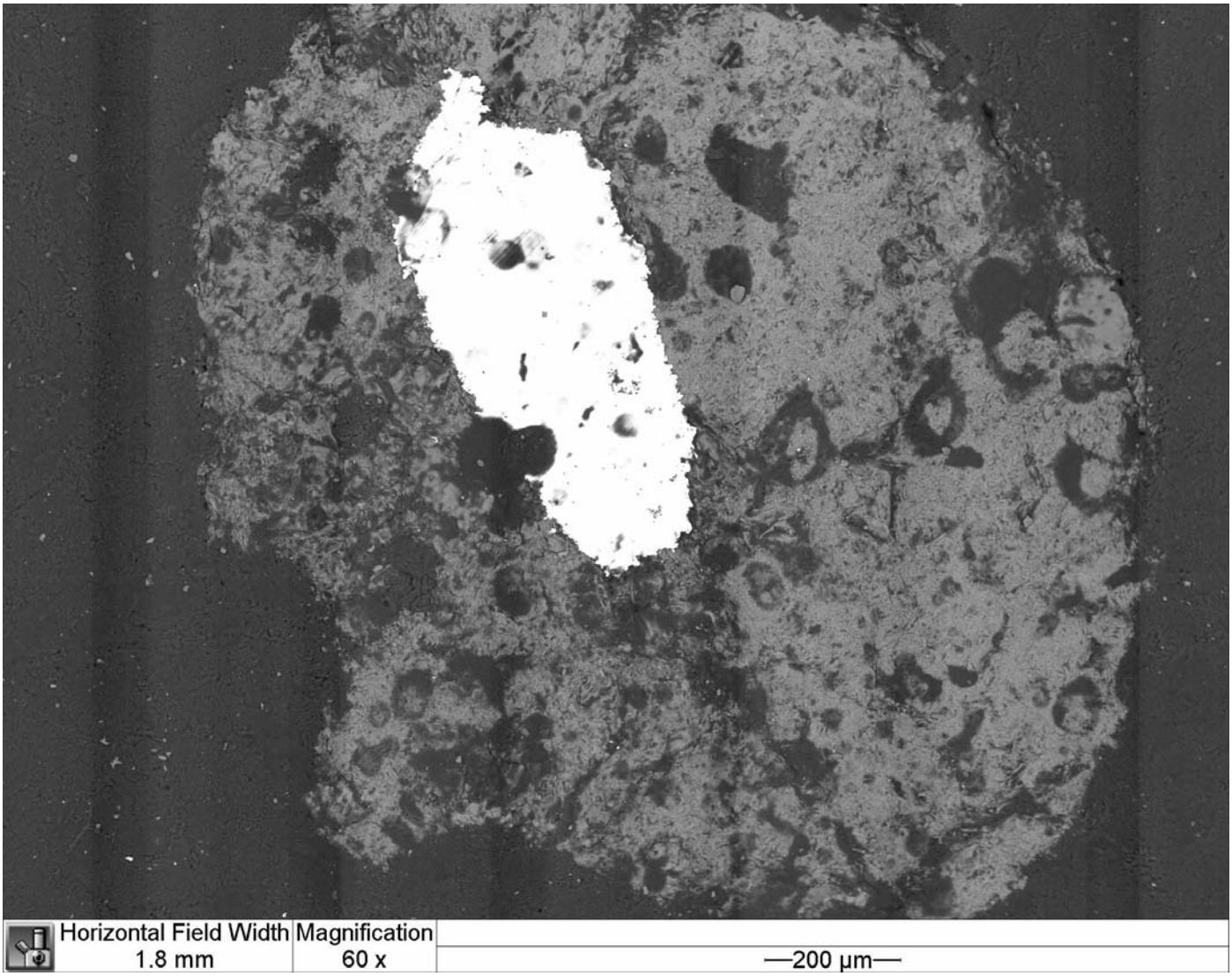

Experiment 11, 95% An_{66} composition. Whole-sample image showing the difficulty in distinguishing crystal from glass. Feldspar crystals were found by blindly analyzing points until a region very rich in Al was found. Glass matrix was found by a similar method but regions with mixed proportions of Al, Mg, Ca, and Na were targeted. Bright white ellipsoidal shape is the platinum used to correctly orient the three samples within one graphite capsule.

Experiment 11

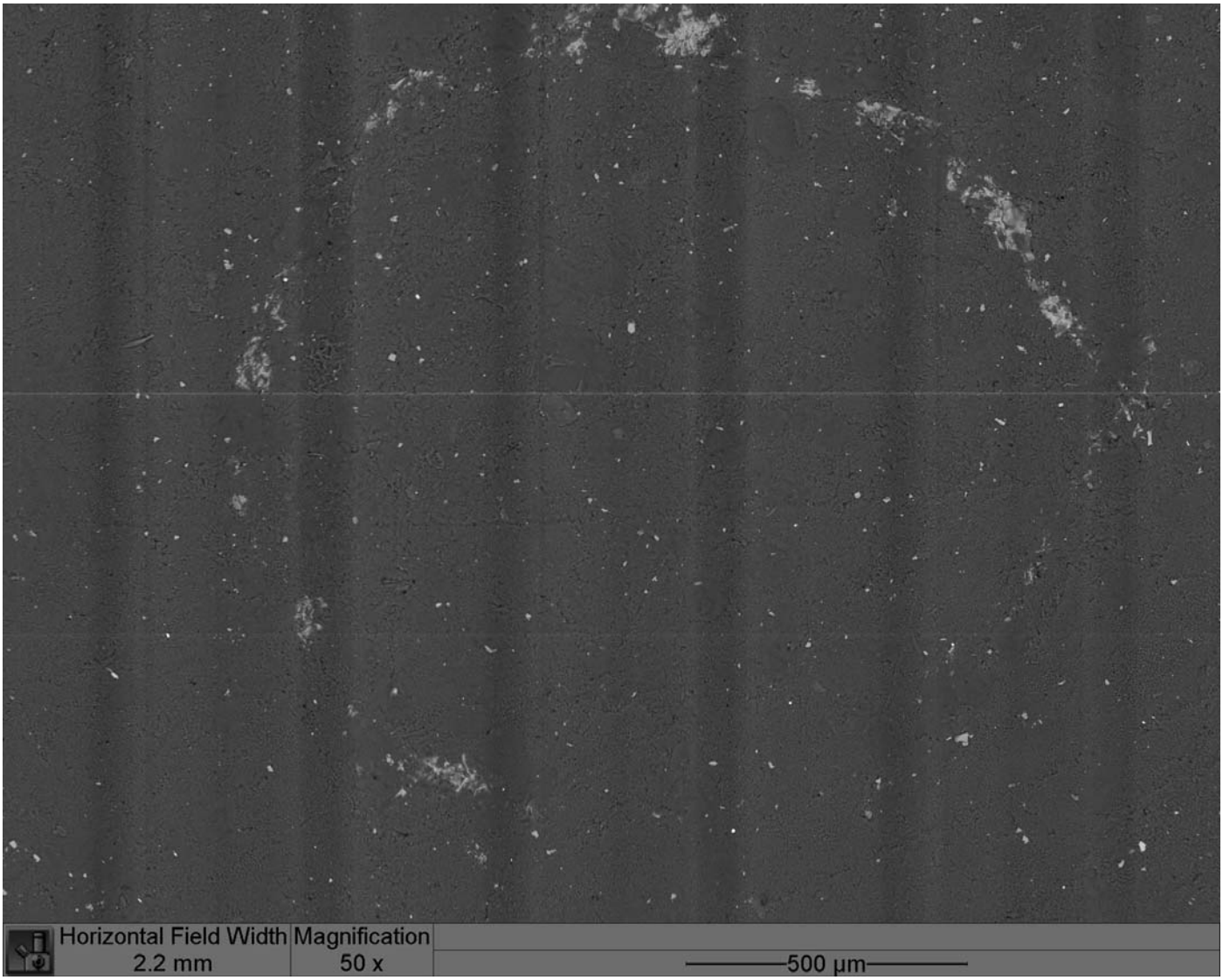

Experiment 11, 60% An_{66} composition. Whole-sample image in which the actual sample is seen by the light grey ring-like shape. The dark grey material is graphite powder that was not ground off. The fragile nature of many of these samples made the polishing process difficult in that some samples were easily destroyed. For this reason, some of the graphite powder was not ground all the way off if enough of the sample was showing to do an analysis. As for the 95% An_{66} composition for experiment 11, it was difficult to distinguish crystal from glass in this sample and so olivine crystals were found as regions free of Al.

Experiment 11

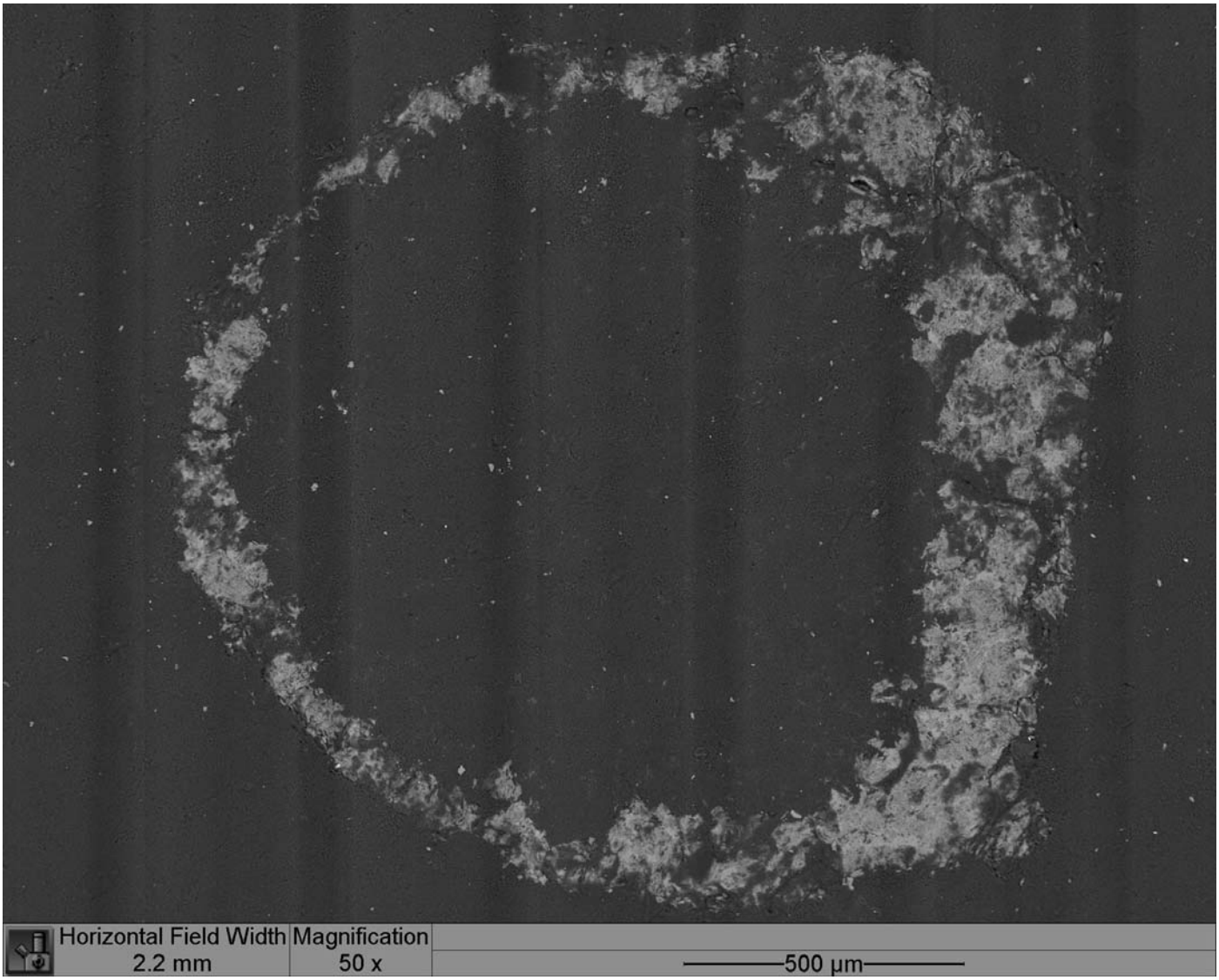

Experiment 11, 20% An_{66} composition. Whole-sample image in which the actual sample is seen by the light grey ring-like shape. The dark grey material is graphite powder that was not ground off. The fragile nature of many of these samples made the polishing process difficult in that some samples were easily destroyed. For this reason, some of the graphite powder was not ground all the way off if enough of the sample was showing to do an analysis. As for the 95% and 60% An_{66} compositions for experiment 11, it was difficult to distinguish crystal from glass in this sample and so olivine crystals were found as regions free of Al.

Experiment 12

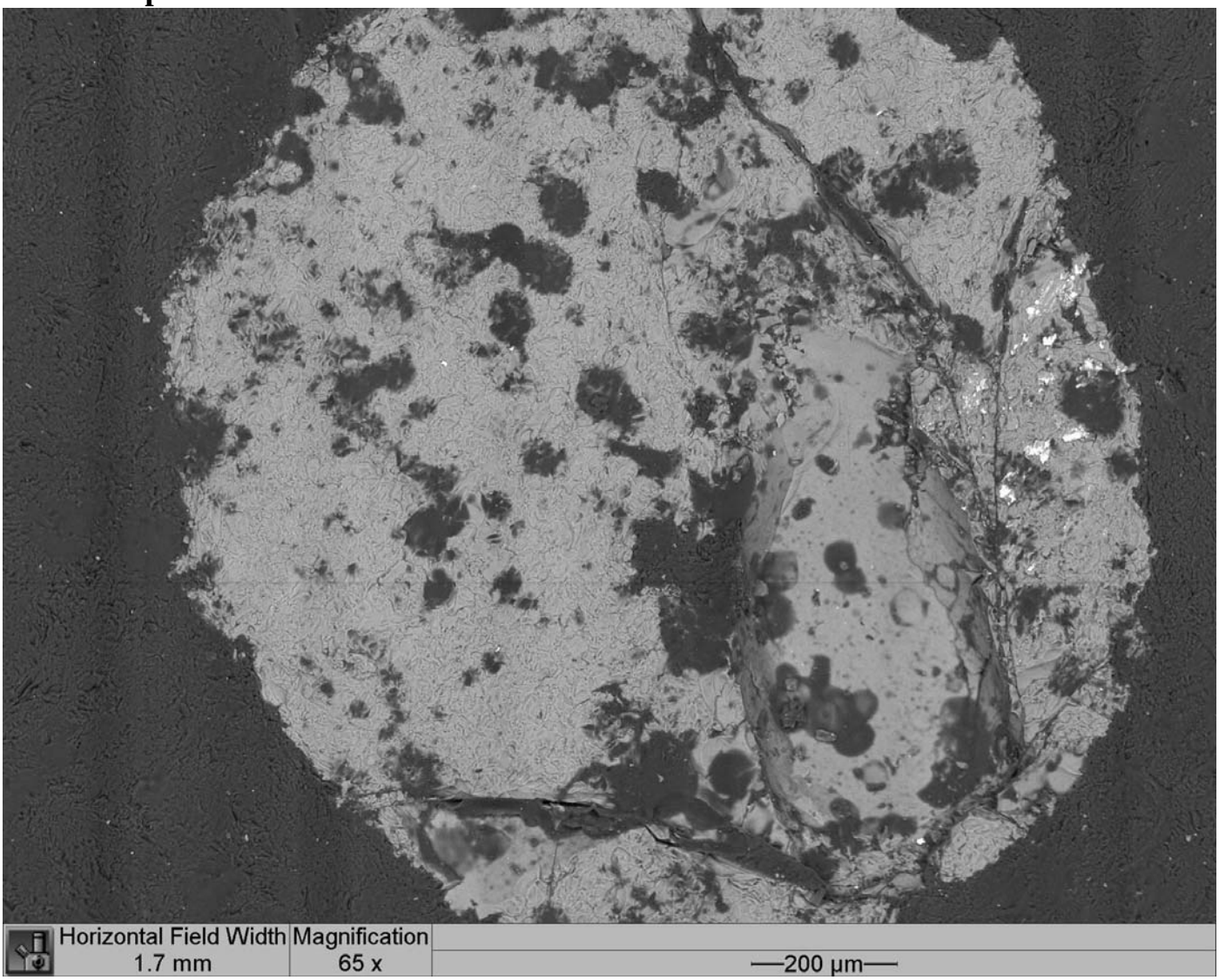

Experiment 12, 95% An_{66} composition. Whole-sample image showing the difficulty in distinguishing crystal from glass. Just as with experiment 11, feldspar crystals were found by blindly analyzing points until a region very rich in Al was found. Glass matrix was found by a similar method but regions with mixed proportions of Al, Mg, Ca, and Na were targeted.

Experiment 12

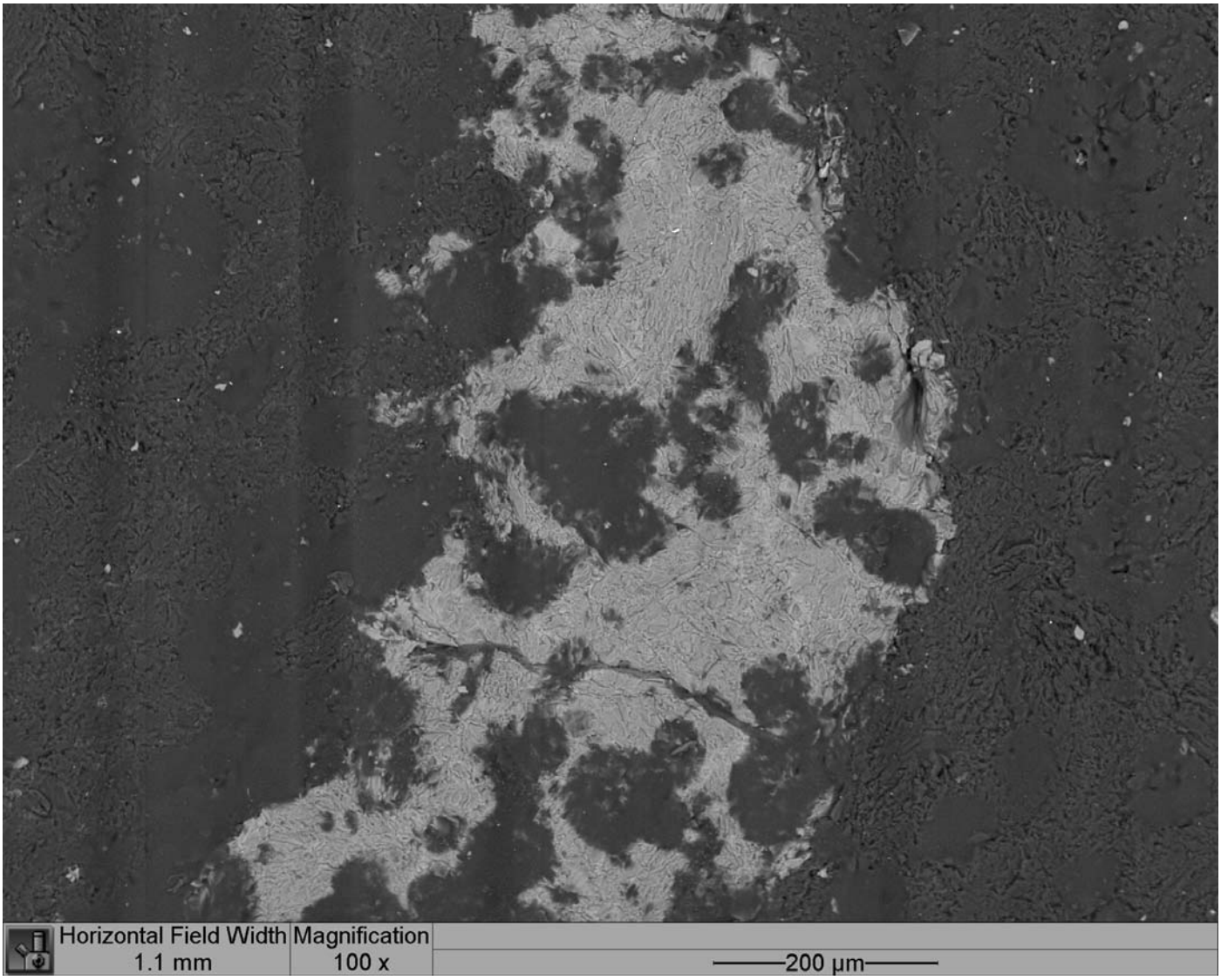

Experiment 12, 20% Ab composition. Whole-sample image showing the difficulty in distinguishing crystal from glass. Just as with experiment 11, olivine crystals were found by blindly analyzing points until a region free of Al was found. Glass matrix was found by a similar method but regions with mixed proportions of Al, Mg and Na were targeted.

Experiment 12

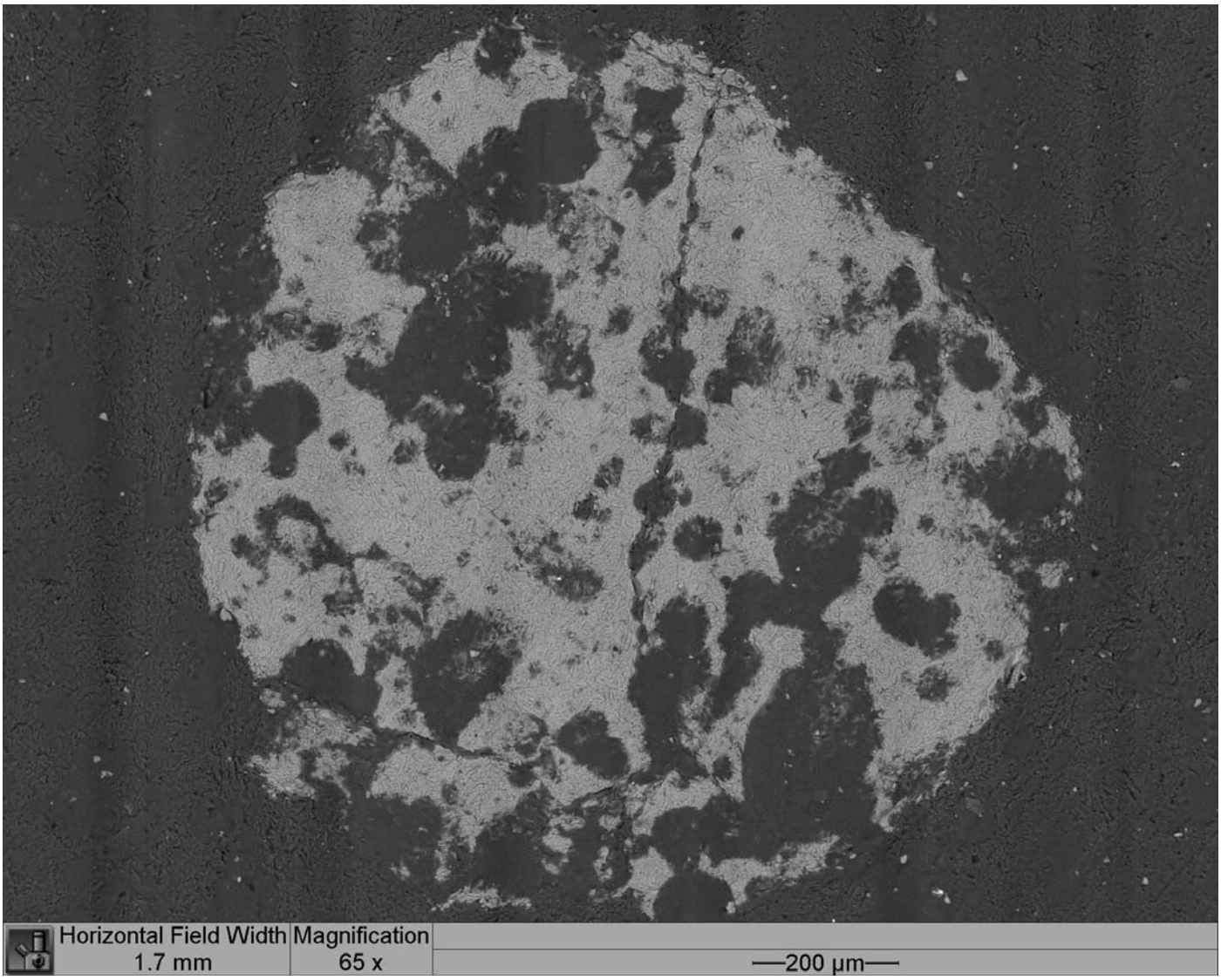

Experiment 12, 20% An_{66} composition. Whole-sample image showing the difficulty in distinguishing crystal from glass. Just as with experiment 11, olivine crystals were found by blindly analyzing points until a region free of Al was found. Glass matrix was found by a similar method but regions with mixed proportions of Al, Mg, Ca, and Na were targeted.